Beam Physics Note
TRI-BN-20-12
September 3, 2020

Maximum Entropy Tomography at the ISAC-RFQ

Olivier Shelbaya

TRIUMF

Abstract: Ongoing work to deploy quadrupole scan tomographic reconstruction methods at TRIUMF's ISAC facility necessitates a working understanding of the relationship between diagnostic inputs and tomographic output. In this report, simulated beam diagnostic readings generated from `TRANSOPTR` are fed to the Maximum Entropy Tomography (MENT) algorithm. Comparison of the tomographically reconstructed beam distributions to the known inputs allows for an evaluation of the relationship between the local tune and the success of attempted reconstructions. Using these insights, the output ISAC-RFQ transverse beam distribution is reconstructed, based on quadrupole scans performed in the ISAC-MEBT section. The RFQ output distributions are finally used to produce a MEBT-DTL drifting beam simulation of an on-line tune from June 2020, found to be consistent with the measured output DTL beam size.

4004 Wesbrook Mall, Vancouver, B.C. Canada V6T 2A3 Tel: 604 222-1047 www.triumf.ca

Contents

1 Motivation for Tomographic Reconstruction at ISAC

Development of model coupled accelerator tuning methods critically depend upon the ability to extract information about the beam distribution at different locations along the machine and its beamlines. This allows for monitoring of machine performance by way of comparison between simulated and measured beam properties. This also enables the development of a diversity of feedback-based tuning algorithms based upon this comparison. However, for deployment on an already-built accelerator lacking a dedicated emittance meter, this presents added costs. One also has to consider the often already crowded beamlines or accelerator lattice may render installation of a supplemental device difficult. This report covers the application of a tomographic method to extract the transverse beam distribution in the ISAC linac from existing diagnostic device measurements only. It is intended to serve as a record of work done to better understand how to perform such a procedure.

In Section 2, a brief overview of the concept of quadrupole scan tomographic reconstruction using beam profile monitors is presented. This is followed by a short review of the sigma matrix/beam matrix formalism in Section 3. Reconstruction of an underlying phase space beam distribution is accomplished in this work using the maximum entropy tomography (MENT) algorithm, which is briefly introduced as well in Section 4. It is important to mention that MENT has been previously validated at TRIUMF by the Beam Physics group [1], in addition to being used elsewhere at TRIUMF such as the proton beamlines, in addition to the electron linac and ARIEL beamlines [2, 3, 4]. In addition, several co-op student projects have revolved around the processing and displaying of MENT reconstructions, which includes quadrupole scans, with written reports available in [5, 6, 7, 8]. It was found in at least some of these projects that difficulty was encountered in defining optimum quadrupole scan intervals, sometimes producing puzzling results. This work attempts to better explore and define a strategy to successfully use quadrupole scan MENT reconstruction.

Section 5 of this report presents an exploration of MENT's functionality using simulated input beam data. For this, the optr companion script `twissify` is used to generate simulated beam diagnostic data which is fed to MENT for reconstruction. This allows for an evaluation of a variety of quadrupole scanning strategies, using `TRANSOPTR`'s speed and flexibility to allow for offline development of MENT reconstruction methods. Throughout the report, a set of guidelines for successful tomographic reconstruction based on quadrupole-scanning is presented, intended as a record for the prospective new user of this technique and its listed tools.

With confidence gained in the functionality of MENT, in Section 6 on-line quadrupole scan tomography measurements are carried out in the ISAC linac's MEBT section, immediately following the RFQ. As an evaluation of the effect of noise reduction and due to the presence of skewness in the profiles, a skew-Gaussian function is used to produce smoothed profiles which approximate the measurements. Both skew-Gaussian processed and raw (noisy) RPM datasets are supplied to MENT, allowing for a comparison of reconstruction result. This allows for a preliminary extraction of the output transverse beam distribution from the ISAC-RFQ.

2 Quadrupole Scanning on a Diagnostic

The effect of a quadrupole on an elliptical particle distribution in position-momentum phase space is a distortion which changes its orientation and aspect ratio. Upon exiting the field, the distribution then drifts apart over time. This is shown in Figure 1, where a conceptual transverse beam envelope exits a quadrupole (red box). In the figure, the ellipses represent the (x, P_x) phase space distribution of the particles comprising the beam. The quadrupole's focal length is represented by a dot in the beam envelope.

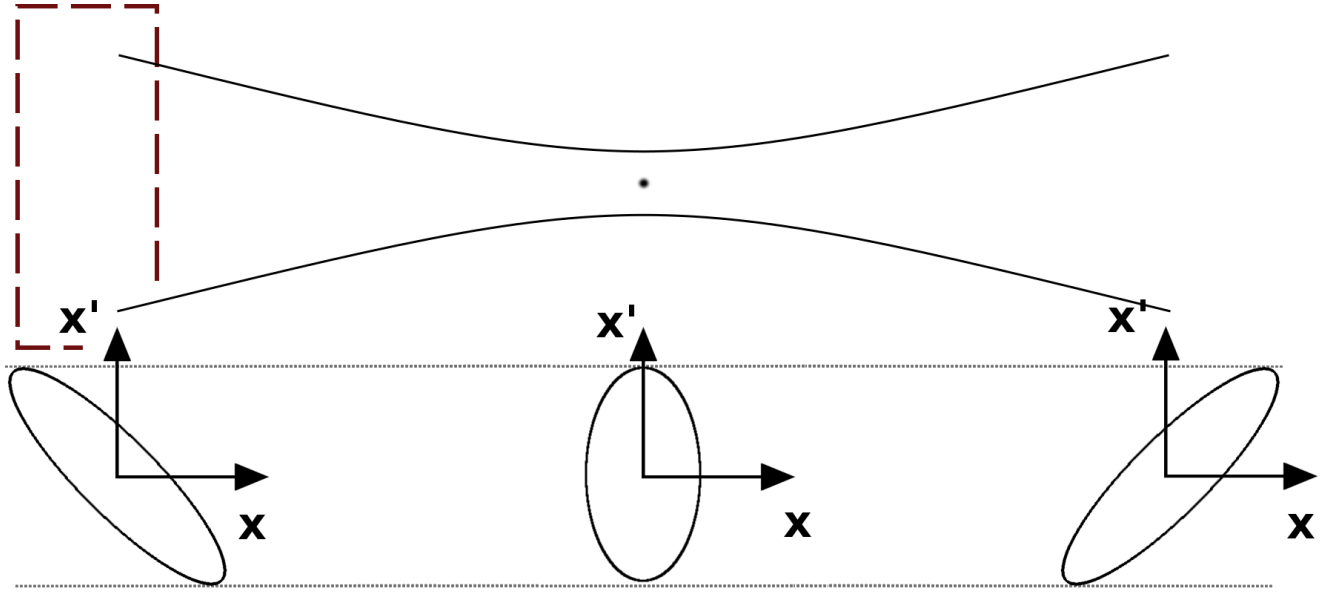

Figure 1: Conceptual beam envelope (top) and associated transverse phase space beam distributions (bottom) for an ion beam extant a focusing quadrupole (red) focused at a point. Beam propagates from left to right. The location of the focal point (centre) depends on the quadrupole field settings. The envelope width is the ellipse projection on the X-axis.

If a diagnostic device, such as a beam profile monitor, is placed some fixed distance downstream of a quadrupole of known physical dimensions and field properties, it is then possible to reconstruct the beam distribution, by recording the beam profile for a series of different quadrupole focal settings: as the quadrupole's effect is varied, the focal point moves with respect to the detector, producing different projections at the location of the diagnostic.

Each beam profile measurement records both of the transverse bunch distributions extent in x and y, which means in principle both transverse distributions can be extracted from a carefully prepared measurement. If the different quadrupole settings are well chosen, the set of imaged distributions will be sufficient for application of a tomographic method to reconstruct the underlying beam distribution. One of the diagnostic images should also include a minimum in beam size vs. quadrupole current. This is crucial as it means the distribution has been imaged at its narrowest aspect, implicitly providing information on the overall distribution's size.

3 Beam Matrices and Moments

Using the sigma matrix formalism for charged particle beams, the distribution at the diagnostic device can be geometrically transformed using the point-to-point transfer matrix $\boldsymbol{\mathcal{M}}$ for an initial beam distribution $\boldsymbol{\sigma_i}$:

$$\boldsymbol{\sigma_f} = \boldsymbol{\mathcal{M}}\boldsymbol{\sigma_i}\boldsymbol{\mathcal{M}}^{\boldsymbol{T}}, \tag{1}$$

where the matrix $\boldsymbol{\mathcal{M}}$ is symplectic and the last matrix is transposed. The beam distribution measurements carried out at the downstream profile monitor provide partial information on the matrix $\boldsymbol{\sigma_f}$. Assuming we are interested in extracting the initial beam distribution:

$$\boldsymbol{\sigma_i} = \boldsymbol{\mathcal{M}}^{-1}\boldsymbol{\sigma_f}(\boldsymbol{\mathcal{M}}^{-1})^{\boldsymbol{T}}. \tag{2}$$

The following useful relationships are also noted for the x (horizontal) dimension [9]:

$$\sin(\chi) = r_{12}, \tag{3}$$

$$\epsilon_x = x_m P_{xm} \cos(\chi) \tag{4}$$

where (x_m, P_{xm}) are the maximum (x, P_x) projections in phase space and ϵ_x is the emittance. The angle χ is the correlation angle of the distribution in (x, P_x). A note of caution is warranted: depending on the units of (x, P_x), the aspect ratio may be such that the angle χ does not correspond to a geometric tilt. This is only true if the (x, P_x) axes have a 1:1 correspondence. The statistical moments of the distribution are also of key interest. For a distribution of N particles in (x, P_x, y, P_y, z, P_z) phase space, the first moment for the x-coordinate, corresponding the mean or centroid in x, is given by:

$$\langle x \rangle = \frac{1}{N} \sum_{i=1}^{N} x_i, \tag{5}$$

while the second moment, which measures the spread or variance, is:

$$\langle x^2 \rangle = \frac{1}{N} \sum_{i=1}^{N} (x_i - \langle x \rangle)^2. \tag{6}$$

For a large particle population, as N grows, the sums can be converted to integrals. The general expression for the i^{th} moment of a distribution $f(x)$ centered about a point c is

$$\mu_i = \int_{-\infty}^{\infty} f(x)(x - c)^i dx, \tag{7}$$

where i is an integer. For this work, we are presently only interested in the first, second and possibly third moments. The latter represent skewness or kurtosis, which measure the asymmetry of the distribution. It is noted that this may eventually be of interest in the matter of beam misalignment quantification.

Taking the square root of (6) produces the root-mean-square (rms) of the distribution, which is used as a measure of the spatial extent the particle ensemble. As an example, for a Gaussian distribution, the 2rms size, centered about the first moment μ, defines a window containing 86% of the particle population. The `TRANSOPTR` computed beam envelope boundary is defined as the 2rms containment in all six canonical coordinate pairs. If the beam is decoupled between spatial dimensions, which is the assumption in this work, the problem reduces to analyzing 2x2 matrices of canonically conjugate coordinates. As an example, for the x-dimension, the elements of the sigma matrix relate to the distribution by:

$$\begin{pmatrix} \sigma_{11} & \sigma_{12} \\ \sigma_{21} & \sigma_{22} \end{pmatrix} = \begin{pmatrix} \langle x^2 \rangle & \langle x P_x \rangle \\ \langle x P_x \rangle & \langle P_x^2 \rangle. \end{pmatrix} \tag{8}$$

This means the rms size of the beam distribution is related to the sigma matrix via:

$$x\mathrm{rms} = \sqrt{\langle x^2 \rangle} = \sqrt{\sigma_{11}} \tag{9}$$

and

$$P_x\mathrm{rms} = \sqrt{\langle P_x^2 \rangle} = \sqrt{\sigma_{22}}. \tag{10}$$

The MENT algorithm implementation used at TRIUMF expects the 4 elements of $\boldsymbol{\mathcal{M}}$ which transforms an unknown initial beam distribution $\boldsymbol{\sigma_i}$ to a partially measured $\boldsymbol{\sigma_f}$ at the beam diagnostic. The location of $\boldsymbol{\sigma_i}$ is arbitrary, so long as it precedes the quadrupole being scanned. For this work, this is by convention the entrance of the quadrupole used for the measurement, however any location connected to $\boldsymbol{\sigma_f}$ by a valid transfer matrix is acceptable, as will be shown.

In order to obtain the elements of $\boldsymbol{\mathcal{M}}$, a beam envelope code can be run in parallel while the measurements are performed. In this case, `TRANSOPTR` [10] is used, which by convention notes the elements of the sigma matrix in normalized form

$$\boldsymbol{\sigma} = \begin{pmatrix} \sigma_{11} & r_{12} \\ r_{12} & \sigma_{22}, \end{pmatrix} \tag{11}$$

with

$$r_{12} = r_{21} = \frac{\sigma_{21}}{\sqrt{\sigma_{11}\sigma_{22}}}. \tag{12}$$

It is critical that the model faithfully reproduce the as-built beamlines and their components, otherwise the elements of $\boldsymbol{\mathcal{M}}$ will be incorrect, which in turn will invalidate the final result. For the ISAC accelerator implementation, which in this note takes place in the MEBT, DTL and HEBT beamlines, a record of the `TRANSOPTR` `acc/` database implementation can be found in [11, 12, 13].

4 Maximum Entropy Tomography

A detailed mathematical description of the maximum entropy algorithm is found in [14] and only a brief overview will be presented in this report. The notation has been kept identical to that of Minerbo.

Tomographic reconstruction refers to the process of recreating an N-dimensional distribution or shape from a collection of (N-1) dimensional projections or images. In the case of the quadrupole-RPM pair, the measurements are one-dimensional beam intensity vs. position, providing the elements of σ_{11} and σ_{33} at the diagnostic. The distribution satisfies the dual criteria:

$$f(x,y) \geq 0 \tag{13}$$

and

$$\int\int_{\mathcal{D}} f(x,y)dxdy = 1. \tag{14}$$

Where $f(x,y)$ is defined on a support $\mathcal{D}$. It is further assumed that there is available a set of projection data G_{jm} which image the function $f(x,y)$ in (N-1) dimensions. These projections are viewed from different projection angles θ_j. The supplied images are constrained to being projections of $f(x,y)$:

$$G_{jm} = \int_{s_0}^{s_1}\int_{t_0}^{t_1} f(s,t)dsdt \tag{15}$$

where the variables (s,t) are related to (x,y) by:

$$x(s,t) = s\cos\theta_j - t\sin\theta_j \tag{16}$$
$$y(s,t) = s\sin\theta_j + t\cos\theta_j \tag{17}$$

.

In other words, the frame (s,t) is rotated about the origin of (x,y) by an angle θ_j, for j distinct projections. The entropy of the distribution $f(x,y)$ is:

$$\eta(f) = -\int\int_{\mathcal{D}} f(x,y)\ln[f(x,y)A]dxdy, \tag{18}$$

A is the area of the support $\mathcal{D}$ over which the function $f(x,y)$ is defined. The term entropy is here understood from the standpoint of information theory, though it also reflects the reality that a

distribution of particles will be in their highest entropy state at any given time. Concretely, MENT iteratively solves the constrained optimization problem:

MENT: Find the distribution $f(x, y)$ subject to the image constraints of Eq. (15) which maximizes η of Eq. (18).

In the words of Minerbo, MENT *"yields the image with the lowest information content consistent with the available data,"* further adding that the method *"avoids introducing extraneous information or artificial structure."* The method is particularly effective for reconstruction with a small number of available images. Applied to the present case of beam dynamics in an accelerator, MENT is used to reproduce an initial beam distribution σ_i which will, after evaluation of Equation (1), most closely reproduce the set of beam profile measurements that are supplied, while maximizing the entropy of Eq. (18). Practically, the MENT algorithm is available at TRIUMF via a library of c++ provided by Y. Rao [15]. The implementation of MENT itself having already been verified in several publications, notably [3], the remainder of this section will focus on the MENT program's required input parameters and a discussion of the performance of the code.

The number of supplied images to MENT should not exceed roughly 10 [14]. The reconstruction is most efficient when provided with a meaningful sampling of the distribution. Keeping the ideal elliptical distribution in mind, this means the dataset provided to MENT should supply to the algorithm implicit information about both semi-axes of the ellipse. In particular, failing to supply MENT with measurements near a minimum beam waist will likely result in an improper estimation of both the distribution's aspect ratio and orientation, in addition to possible artifacts such as filamentation, as will be shown. Of course, one can only be certain of the response of the phase space correlation if the behavior of the beam is known. In other words, selecting an arbitrary current scan domain on an unknown tune is almost guaranteed to fail or produce substantial artifacts.

Finally, it is noted that in TRANSOPTR, relative momenta in the co-moving Frenet-Serret reference frame are treated as angles. As such, for the reconstructions that are to follow, the conjugate coordinate pair (x, P_x) will possess units of length and angle, respectively.

5 TRANSOPTR-Based Algorithm Exploration

The optr-computed transfer matrix $\mathcal{M}$ for the (x, P_x) or (y, P_y) canonical pairs, in addition to the (simulated) RPM measurement from `twissify` are combined to form an MENT compatible data structure. This matrix and RPM sequence are from here on referred to as datapoints. By sequentially running `TRANSOPTR` at different quadrupole values then running the optr companion script `twissify` to generate the diagnostic traces, the final MENT input file is constructed. A short user manual for `twissify` is included in Appendix A. For this case, the MEBT section of the ISAC-I accelerator is used as the eventual goal is to perform an on-line measurement in that section. This offline practice run should also provide insight into the rough quadrupole current range that will be needed.

Beam consisting of $^{20}Ne^{4+}$, exiting the ISAC-RFQ at an energy of 3.06 MeV was simulated up to the location of MEBT:RPM5, downstream of the quadrupole MEBT:Q5, which is the pair used for the quadrupole scan. The 2rms (x,y,z) envelopes are shown in Figure 2. The longitudinal envelope confirms that the 3-gap bunch rotator cavity is on and properly set, producing a longitudinal focus just downstream of MEBT:RPM5. The computation in Figure 2 is based on a mix, using design starting beam parameters along with an operational tune for the quadrupoles in use as of July 2020. The bunch rotator's amplitude and phase were manually set to produce a z-focus at MEBT:FFC5. While the on-line beam envelope is probably not exactly as shown in the figure, it nevertheless should be similar.

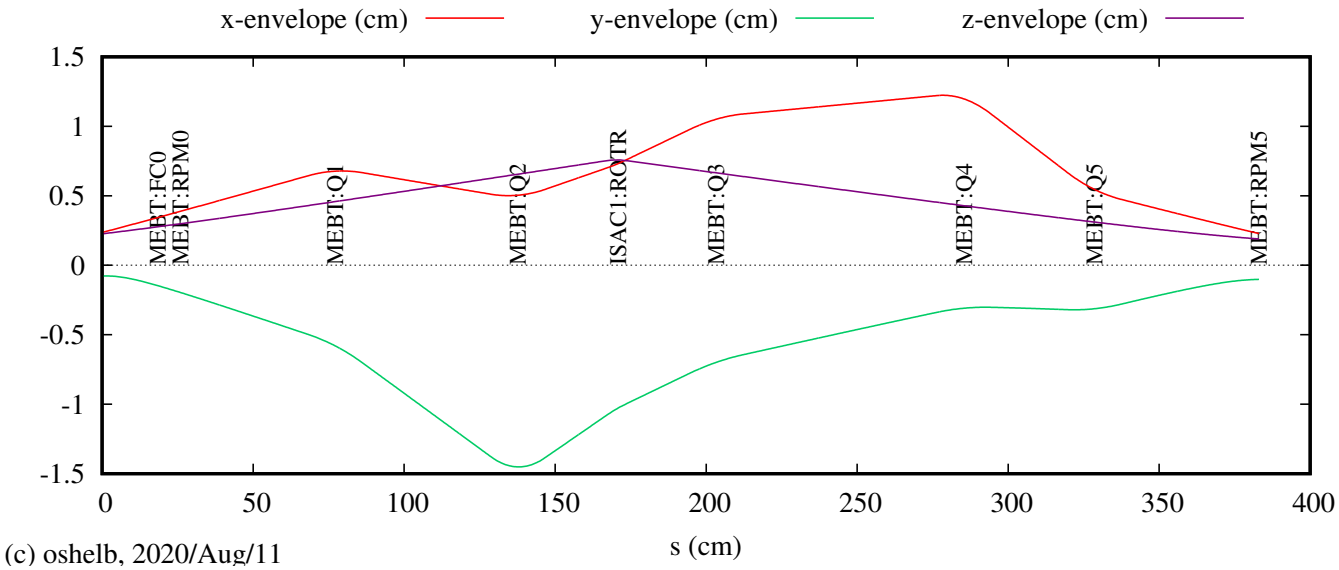

Figure 2: `TRANSOPTR` computed 2rms (x,y,z) beam envelopes at exit of ISAC RFQ, propagating from left to right. In this test, MEBT:Q5 and RPM5 are used. Sequence generated from `acc/` database implementation in [11].

5.1 Tune Considerations and Quadrupole Scan Range

Experience so far has shown that simply attempting an arbitrary quadrupole scan is a recipe for frustration, which devolves into 'hunting' for suitable intervals. That the tune's behavior at a quadrupole diagnostic pair needs to be known to some degree before a measurement poses somewhat of a circular constraint: One must have at least some knowledge of the tune beforehand, to best identify where and how exactly can tomographic reconstruction be performed.

Figure 3 shows two `twissify` generated initial optr beam distributions for x (horizontal) and y (vertical). These distributions correspond to the starting $\boldsymbol{\sigma_i}$ used in sequential `TRANSOPTR` runs from MEBT:Q5 to RPM5. In a real on-line measurement, the distributions of Figure 3 would be unknown and finding them the object of the exercise. For this, the quadrupole current was scanned in order to find a suitable quadrupole range for the measurement. The resulting beam envelopes for the range [0,20]A are shown in Figure 4, left. The current range is promising due to the meaningful change in values for (r_{12}, r_{34}) for the x and y distributions. Ensuring the quadrupole scan interval features this variation will provide MENT with a proper set of imaging angles θ_i of the distribution, maximizing chances of success.

The `TRANSOPTR` envelope simulations covering the [0,20]A range on Q5 were used to generate simulated, noise-free Gaussian profiles featuring the rms width of the beam. These simulated profile measurements are shown in Figure 4, right. The quadrupole scan's effect on the correlation parameters (r_{12}, r_{34}) is shown in Figure 5, left. The right side of the figure shows r_{ij} versus the 2rms beam sizes for x and y, with Q5 currents labeled.

The quadrupole scan must include datapoints for which the 2rms size of the beam on the diagnostic monitor is at a minimum, which will provide MENT with information about one of the ellipse semi-axes. In order to scan through a minimum beam width in x, MEBT:Q5's current should be varied from about 4A to 8A, while for y the scan interval needs to be expanded from about 4A to 14A. Moreover, both minimum waists in (x,y) do not occur at the same quadrupole current. For this reason, it may not be possible to reconstruct both x and y from the same quadrupole scan.

The exercise has thus far shown that it is instructive to have an initial tune simulation at hand. In the present example, the range [0,20]A for MEBT:Q5 will be used for $^{20}Ne^{4+}$ at RFQ output energy during the on-line portion of the measurement. Given that ISAC-MEBT quadrupoles have current ranges of [0,60]A, this has divided the range of Q5 currents to work with by 3. This is time that does not need to be spent hunting for ideal scan intervals when performing on-line tests, for which time is limited. If the on-line behavior of the tune is found to significantly disagree, it will further provide strong evidence of a disagreement with the design tune assumption shown in Figure 2.

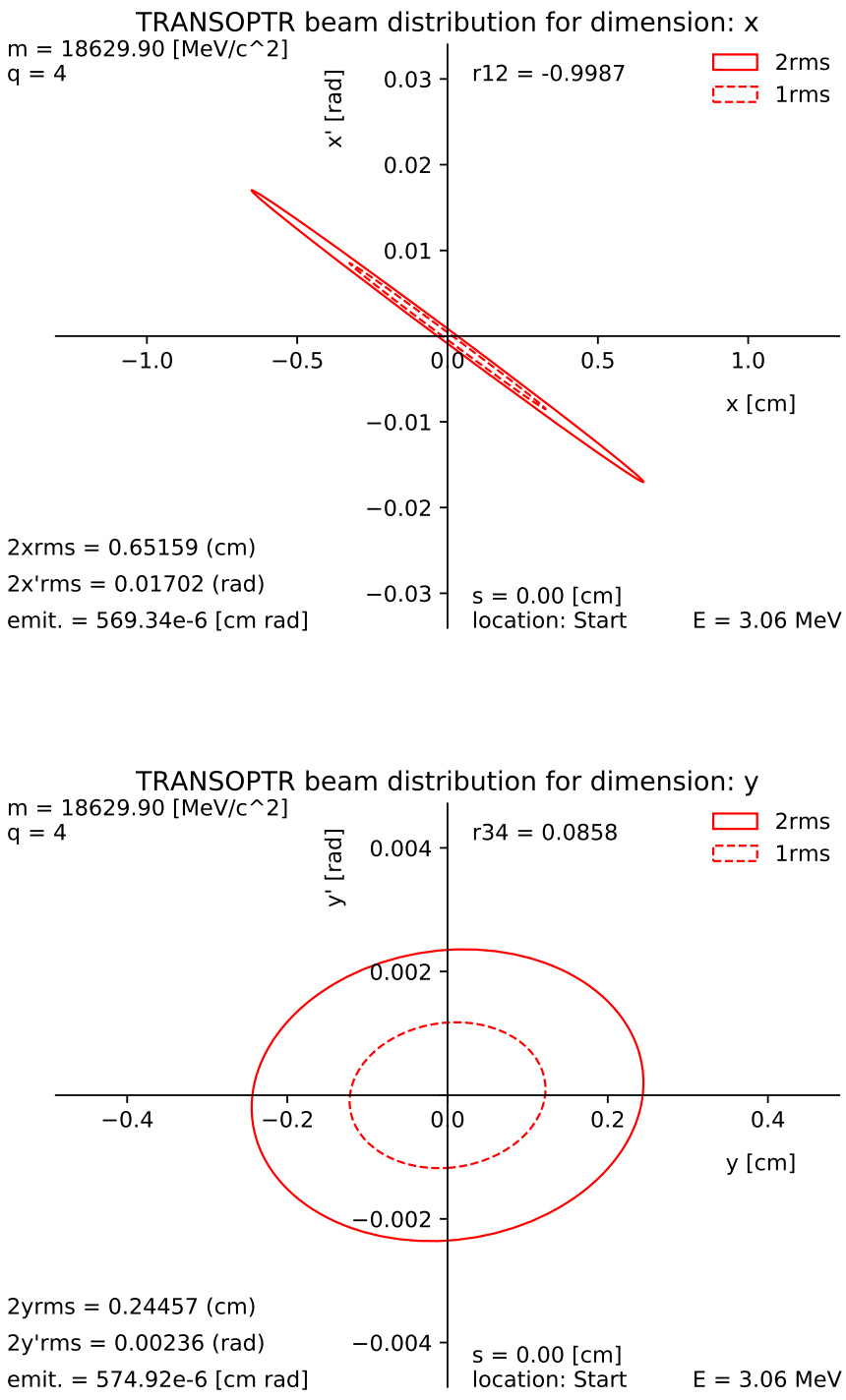

Figure 3: **Top:** `TRANSOPTR` initial beam containment ellipses for the x-dimension (horizontal), at the entrance of MEBT:Q5. **Bottom:** corresponding y-distribution (vertical). `twissify` has been used to generate simulated Gaussian RPM traces. These two distributions are used for the remainder of this work as starting parameters for `TRANSOPTR` beam simulations.

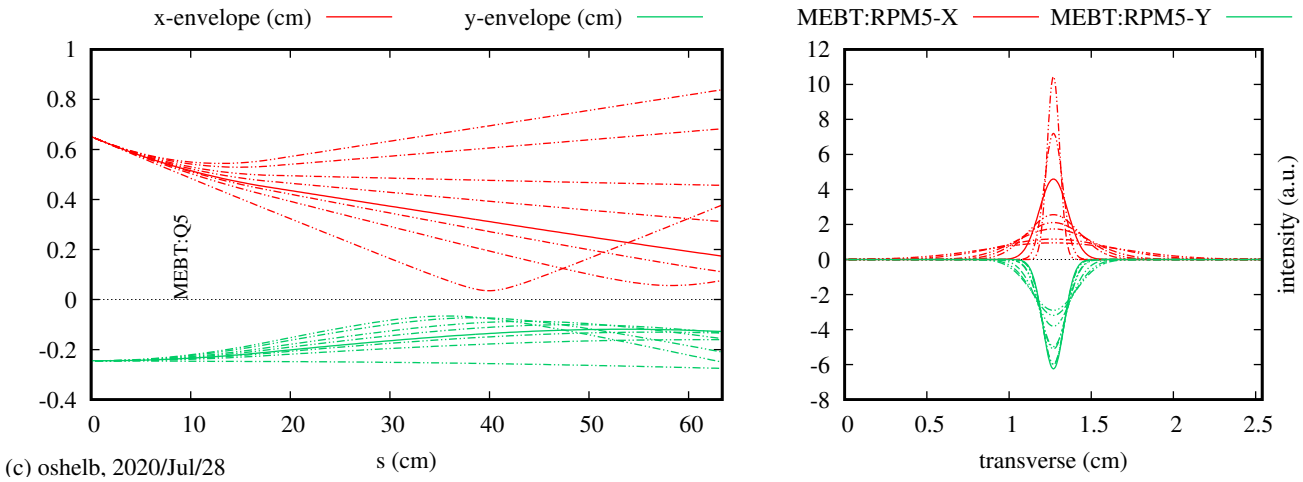

Figure 4: **Left:** swarm of `TRANSOPTR` computed 2rms (x,y) envelopes starting at the entrance of MEBT:Q5 and terminating at MEBT:RPM5, obtained by scanning the quadrupole from 0 to 20A. **Right:** Corresponding `twissify` generated Gaussian RPM profiles with $\sigma = 0.5\sqrt{\sigma_{11}}$, from `fort.envelope`.

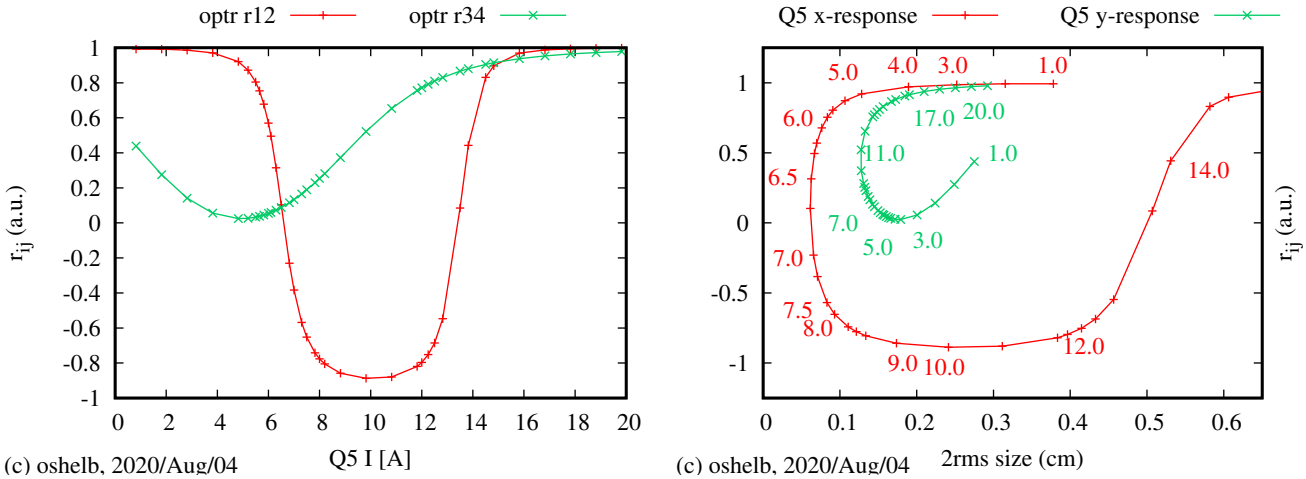

Figure 5: **Left:** `TRANSOPTR` computed correlation coefficients r_{12} and r_{34} associated with the MEBT:Q5 quadrupole scan shown in Figure 4. **Right:** Plot showing r_{ij} versus 2rms beam size for x and y. The MEBT:Q5 current in [A] corresponding to each point is labeled on the graph.

5.2 Initial MENT Reconstruction

The initial test simply consists of attempting a successful reconstruction of the optr distributions shown in Figure 3. The command `twissify -t` is used to generate simulated MENT formatted entries, which include the MEBT:Q5 to RPM5 transfer matrix. See Appendix A for more details on this procedure. Two initial quadrupole scans are performed, one for each dimension. Within the expected Q5 [0,20]A current range, Q5 was roughly set to produce a minimum beam width, looking to Figure 5, right. Remaining datapoints were taken about this minimum. Quadrupole scans which best reconstructed the input distribution were found by asking:

At which quadrupole current I_0 is the value of $|r_{ij}|$ at a minimum? This should roughly define the midpoint of the quadrupole scan in a plot of r_{ij} vs 2rms size (Fig. 5, right).

For the horizontal case the range [4,8]A was used, while for the vertical it was [5,20]A. Initially, both quadrupole scans were performed with 8 samples, all equidistantly spaced. The resulting MENT reconstructions are shown in Figure 6, qualitatively producing good agreement with the inputs from Figure 3.

It is important to remember that the perceived tilt of the ellipse also depends on the plotting scale that is used. For a quantitative measure of the reconstruction's agreement with the simulated starting beam, a modified version of the script `general_contour_plot.py` [8] was used. In brief, the script accepts the MENT reconstruction output file `TOMO_FIT.DAT` and computes the moments of the distribution, which is then plotted along with information about the distribution.

Comparison of the MENT reconstructed beam parameters with the starting `TRANSOPTR` 2rms values in Figure 3 shows good agreement. Concretely, the optr values for the extent of the (x, P_x, r_{12}) and (y, P_y, r_{34}) distributions were (6.52mm,17.02mrad,-0.9987) and (2.45mm,2.36 mrad, 0.086) respectively. Post processing of the MENT output returned values of (6.52mm,17.02mrad,-0.9981) and (2.48mm,2.35mrad,0.0766) for the x and y dimensions. `TRANSOPTR` (x,y) emittances were (5.69,5.75)μm, with MENT producing (6.80,5.81)μm. It is noted that the x-emittance is significantly off from the input, which was always the case regardless of quadrupole scan strategy.

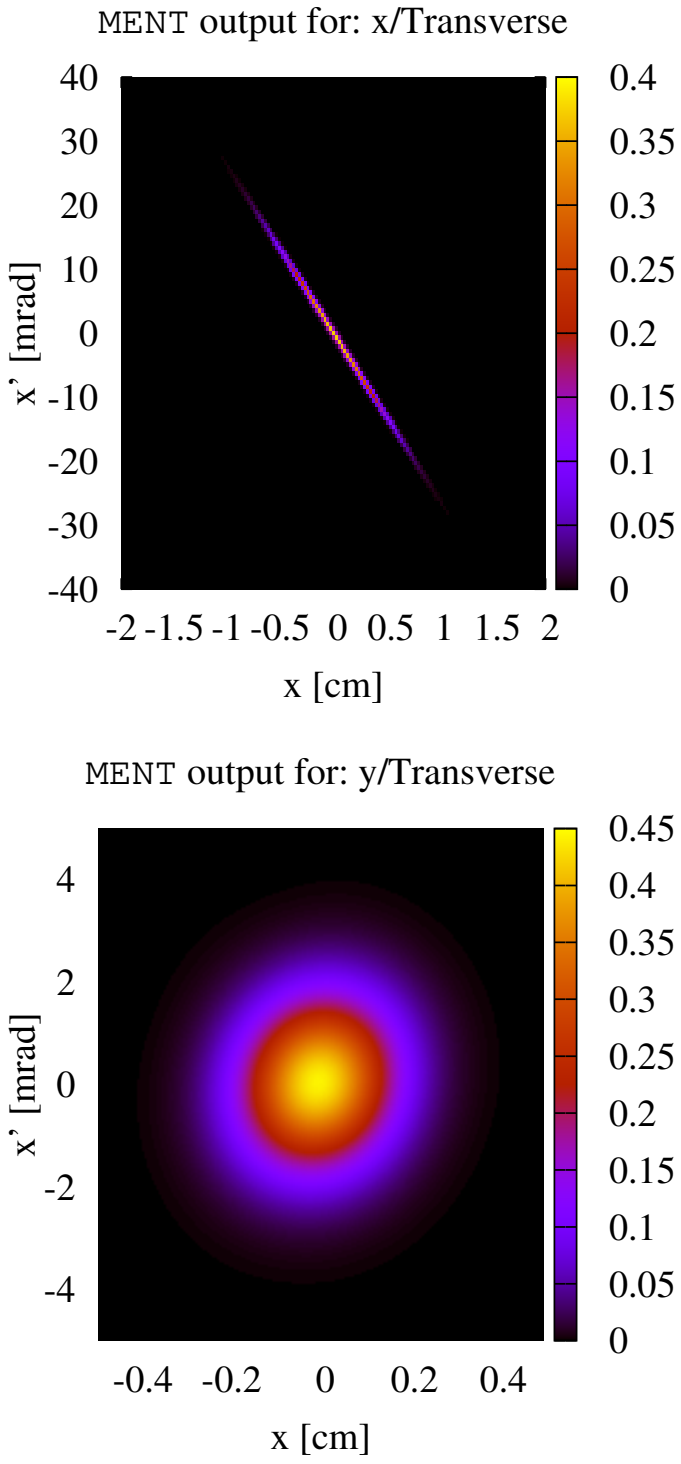

Figure 6: MENT reconstruction of the initial beam ellipses (Fig. 3) for (x,y), using `twissify` generated simulated Gaussian RPM traces at MEBT:RPM5.

5.3 Exploring Quadrupole Scan Intervals

To better understand how to perform a successful quadrupole scan measurement, this section will show the MENT output results for different quadrupole scans using the same simulated starting distribution of Figure 3. What is intended to be demonstrated is the importance of carefully selecting the current scan range and spacing, which involves at least elementary knowledge of the local tune. While this section does not present an exhaustive investigation of the relationship between tune, scan interval and result, from a few different sampling strategies, a clear pattern should emerge.

After several different trials, it was found that the initial 8 datapoint scans from the previous section provided little added benefit but were more time consuming. Five datapoint scans were found to be both easy to perform and sufficient to produce good agreement. To this end, a series of 5-RPM based simulated quadrupole scans were performed for a variety of quadrupole current setting incrementation strategies. Figure 7 shows three separate results with differently spaced current step sizes, each of which illustrate the sensitivity of the MENT reconstruction on the supplied data. The simulated quadrupole scans from this point on are labelled QS-i, i=1,2,3,.. In Figure 8, two further 5-point quadrupole scans were performed, this time ensuring that the scan iterated through a minimum for beam size for x (top of figure) and a minimum for y (bottom of figure).

When using MENT, supplying more datapoints does not necessarily equate a better output.

The script `general_contour_plot.py` was then used to compute the rms sizes of each reconstructed distribution. This is listed in Table 1. It is clear that varied quadrupole scan sampling has an effect on the reconstruction's output. In particular, the coefficient r_{34} changes considerably across the scans. None of the x-reconstructions successfully recreate the x-emittance, without errors well above 10%.

Label	2xrms [mm]	2x'rms [mrad]	r_{12}	ϵ_x [μm]	2yrms [mm]	2y'rms [mrad]	r_{34}	ϵ_y [μm]
TRANSOPTR (Fig. 3)	6.52	17.02	-0.9987	5.69	2.45	2.36	0.0858	5.75
QS-1 (Fig. 7, top)	6.52	17.02	-0.9982	6.68	3.16	2.42	-0.1191	7.59
QS-2 (Fig. 7, mid.)	6.52	17.02	-0.9983	6.51	2.49	2.35	-0.1191	5.83
QS-3 (Fig. 7, bot.)	6.49	16.93	-0.9982	6.55	3.35	2.22	0.0291	7.46
QS-4 (Fig. 8, top)	6.52	17.03	-0.9979	7.13	3.81	2.78	-0.4045	9.67
QS-5 (Fig. 8, bot.)	6.50	16.97	-0.9984	6.14	2.45	2.36	0.0857	5.75

Table 1: MENT reconstruction of TRANSOPTR simulated quadrupole scans shown in Figs. 7 and 8. Optimum x and y quadrupole scans, found to agree most closely with the original TRANSOPTR distribution, are highlighted in green.

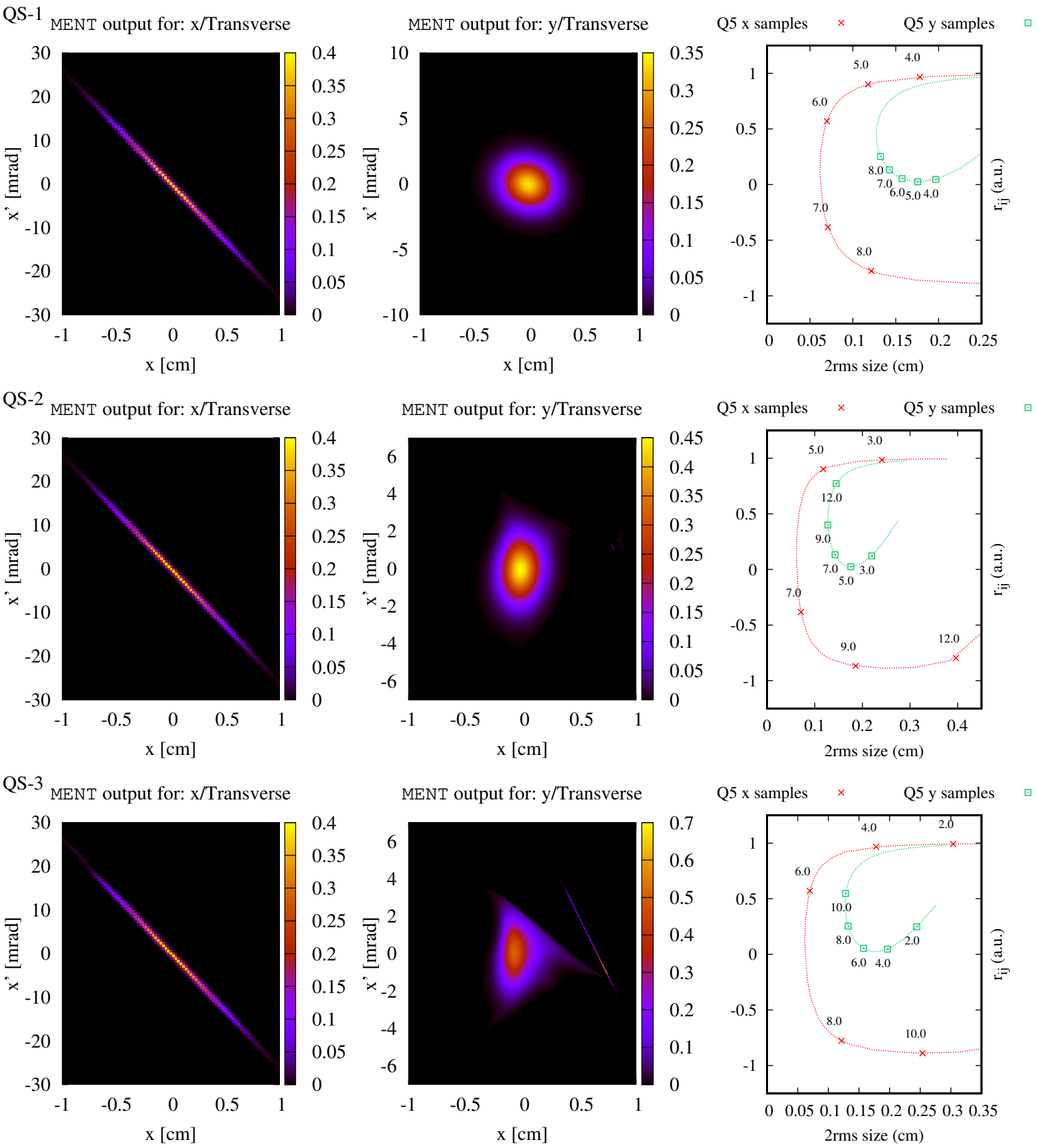

Figure 7: Sequence of 5-datapoint simulated RPM-based MENT reconstruction of TRANSOPTR generated beam distribution of Fig. 3. The reconstructions for x (**Left**), y (**Centre**) and the quadrupole scan plot (**Right**) are shown line by line, from top to bottom. Quadrupole currents are labeled on the right-hand graph.

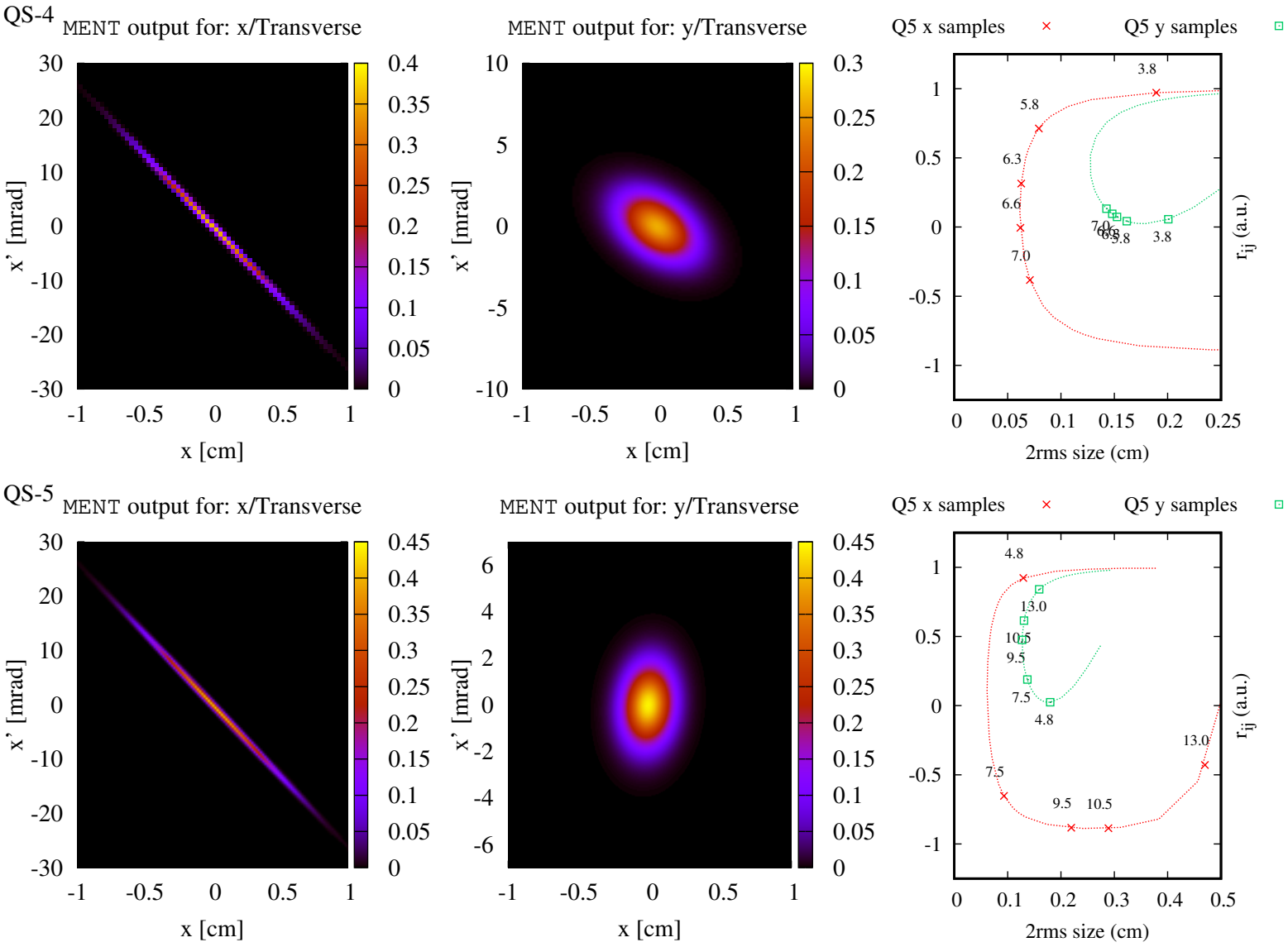

Figure 8: Sequence of 5-datapoint simulated RPM-based MENT reconstruction of TRANSOPTR generated beam distribution of Fig. 3. The reconstructions for x (**Left**), y (**Centre**) and the quadrupole scan plot (**Right**) are shown line by line, from top to bottom. Quadrupole currents are labeled on the right-hand graph.

Importantly, in Table 1, quadrupole scans QS-1 to QS-4 have failed to simultaneously recreate the input y-distribution's size, orientation and emittance. This includes quadrupole scans that feature a minimum r_{34} (QS-2 and QS-3) as a function of the vertical 2rms size, hinting that there is another consideration that has been missed:

On either sides of I_0, which features the minimum $|r_{ij}|$ value in the set, the quadrupole scan should feature a monotonously increasing $|r_{ij}|$ as a function of the 2rms beam size. This will avoid involuntarily introducing degenerate images.

Providing MENT with images featuring very similar r_{ij} values but different 2rms beam sizes has been found to consistently lead to streaking, deformation and other artifacts. This tune dependent effect can be thought of as providing projections which conflict with the remainder of the set, generally causing an increase in the area of the reconstructed distribution and compromising the rms sizes of the beam. Scans QS-2 and QS-3 are examples of such conflict for the y-dimension: the r_{34} values start decreasing again as the 2rms beam size increases.

5.4 Optimum Quadrupole Scan Intervals

Which quadrupole scan strategy, given this present tune and these five separate samples, was the optimum for x and y? Looking at Table 1, while it is clear that the sampling strategy from scan QS-5 produced the optimum result for the y-dimension, the picture is less clear when it comes to the distribution in x. The x-measurements are consistently better in terms of the resulting (x, P_x, r_{12}) values, given the broad spatial extent of the ellipse and its eccentricity. However, none of the quadrupole scans performed seem to successfully reproduce ϵ_x. In fact, it was found that reconstructing the emittance of a highly eccentric ellipse was more difficult for the algorithm.

The local transverse beam distribution at quadrupole scan tomographic locations should not possess high values of $|r_{ij}|$. This will compromise MENT's ability to efficiently extract the emittance. Should such an ellipse be unavoidable, analysis suggests the reconstructed 2rms sizes of the distribution may closely agree with the underlying distribution, at the expense of r_{ij} and the emittance.

One must carefully consider the shape of the distribution function $f(x, y)$ that MENT is trying to recreate and the tune. Since the y-distribution is less eccentric than x, it does not display as strong of a peak intensity variation in any of the datasets. In other words, it is possible to miss the quadrupole current producing the narrowest beam size if the current step size is too big. When the quadrupole scan fails to include the minimum width of the distribution, the reconstruction fails to properly recreate the area and correlation angle.

Figure 9 shows a comparison between projections for $f(x, y)$ with the `twissify` RPMs from `TRANSOPTR`. These two datasets are the best horizontal and vertical reconstructions (Table 1). A further verification of the result's validity can be done by checking the MENT reconstruction's projections, comparing them with the original RPM measurements. Concretely, this is done by plotting the output files `FIT_RESULT.DAT` and `TOMO_PROFILES.DAT`. Observe how measurement QS-2 has faithfully reconstructed each of the y-projections (Fig. 9, top left), though inspection of Table 1 shows the y-reconstruction has failed. Not understanding the local tune would preclude this conclusion.

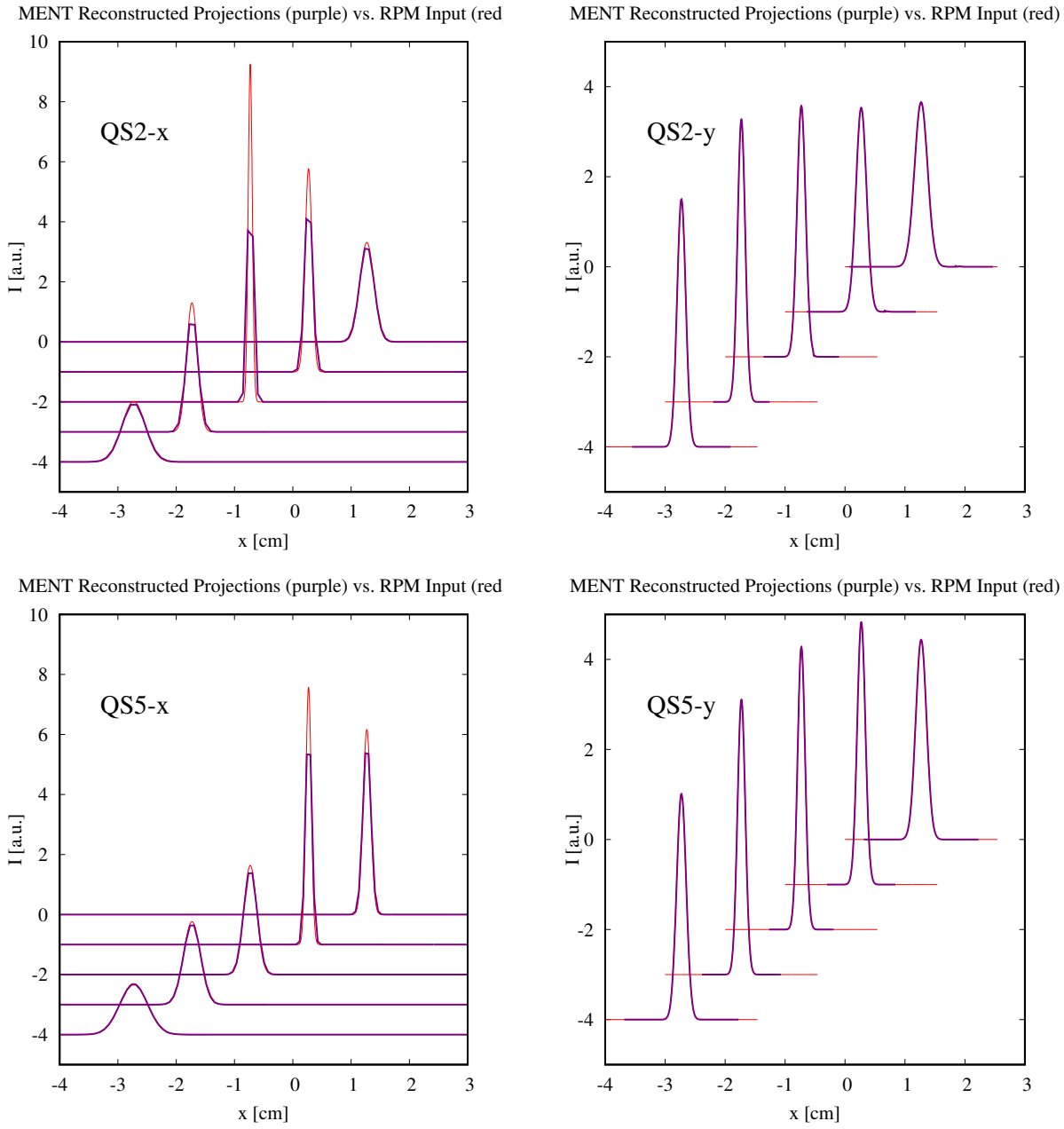

Figure 9: Projections of reconstructed MENT profiles vs RPM readings for QS-2 (**Top**) and QS-5 (**Bottom**). In both cases, the `twissify` simulated RPM data is shown in red, while the projection of the MENT reconstructed $f(x, y)$ is shown in purple. Each dataset has been vertically and horizontally offset by an arbitrary amount for plotting purposes.

5.5 Small Dataset Reconstruction Example

When in doubt, providing a higher number of images does not necessarily equate a better outcome. On the contrary, given what has been discussed to this point, there is a good chance that selecting quadrupole currents at random, for an unfamiliar tune will not satisfy all of the conditions presented thus far. Understanding that providing the correct set of images and projections will enable an accurate reconstruction that fully exploits MENT's power, two examples are presented. Figure 10 shows two quadrupole scan results, both taking only 3 RPM samples. The resulting MENT output are listed in Table 2, with the optimum reconstruction results highlighted in green.

The demonstration of 3 datapoint reconstructions shows that for a well chosen quadrupole scan sampling interval, MENT can effectively reconstruct the entire transverse beam distribution in one measurement. It is better to study the tune and identify an optimum strategy than to attempt measurements with many samples.

The optimum scan interval is tune dependent and should be carefully considered for each quadrupole-scan tomographic reconstruction measurement attempt.

Proposed quadrupole-scan tomographic reconstruction locations should be simulated offline for initial analysis, as done in the present report. This will help establish a theoretical optimum quadrupole scan strategy, given the particularities of the local beam envelope and tune. It will also allow for a more confident identification of any nonstandard behavior during on-line measurements.

Label	2xrms [mm]	2x'rms [mrad]	r_{12}	ϵ_x [μm]	2yrms [mm]	2y'rms [mrad]	r_{34}	ϵ_y [μm]
TRANSOPTR (Fig. 3)	6.52	17.02	-0.9987	5.69	2.45	2.36	0.0858	5.75
QS-6 (Fig. 10, top)	19.83	52.19	-0.9998	20.23	4.59	4.05	-0.8561	9.61
QS-7 (Fig. 10, mid.)	6.52	17.02	-0.9981	6.80	2.48	2.35	0.0766	5.81
QS-8 (Fig. 10, bot.)	7.00	17.92	-0.9978	8.26	2.45	2.36	0.0856	5.75

Table 2: MENT reconstruction of TRANSOPTR simulated quadrupole scans shown in Fig. 10. Both scans feature only 3 images. Optimum x and y quadrupole scans, found to agree most closely with the original TRANSOPTR distribution, are highlighted in green.

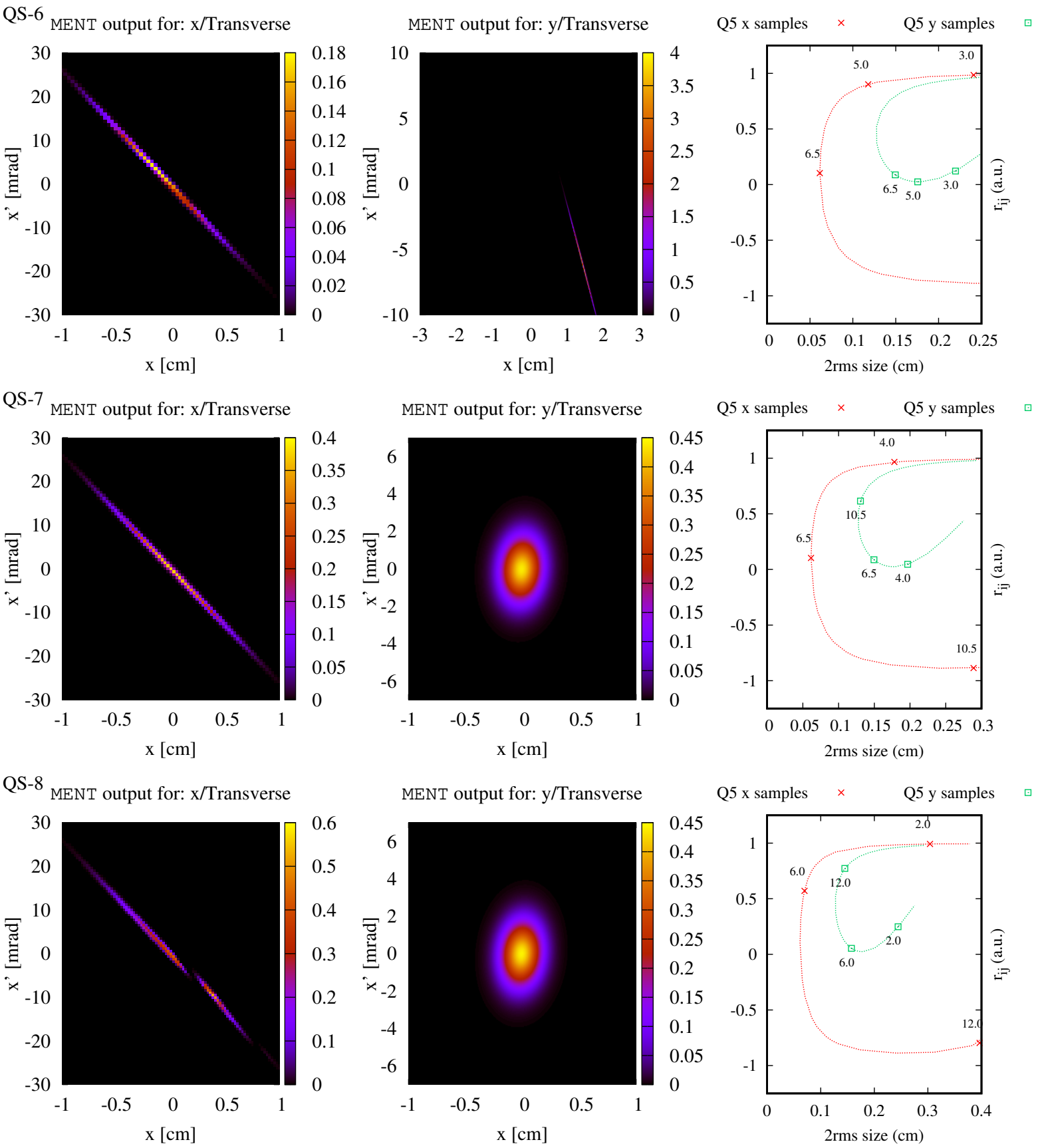

Figure 10: Sequence of 3-datapoint simulated RPM-based MENT reconstruction of TRANSOPTR generated beam distribution of Fig. 3. The reconstructions for x (**Left**), y (**Centre**) and the quadrupole scan plot (**Right**) are shown line by line, from top to bottom. Quadrupole currents are labeled on the right-hand graph.

6 Tomographic Reconstruction of ISAC-RFQ Output

This report ends with an on-line quadrupole scan MENT reconstruction, using the insights that have been gained so far. The simulated measurement in MEBT that has been discussed, was performed on-line during beam development tests on the ISAC accelerator, in June 2020. As in the simulations, a beam of $^{20}Ne^{4+}$ extant the RFQ at 3.06MeV was used. Beam was initially tuned to MEBT per standard procedure, at which point quadrupole scan measurements began. Samples of the raw MEBT:RPM5 traces are shown in Figure 11, with the y-profile on the left hand side and x on the right. It is noted that operational MEBT tunes make consistent use of steering [16]. The RPM profiles that were measured featured prominent skewness when Q5 was detuned from its minimum beam size setting.

The raw data from the RPM readings consists of two arrays. One contains the intensity vs time signal and the other position vs time for the device as it sweeps through the beam. Initial processing consisted of splitting the measurements into x and y datasets containing only the relevant part of the trace. The RPM calibration is such that the x and y traces are always clearly separated. The arrays were cut at their midpoints, producing two equally sized datasets with the transverse profiles. This is roughly the 1” mark in the x-axes of Figure 11.

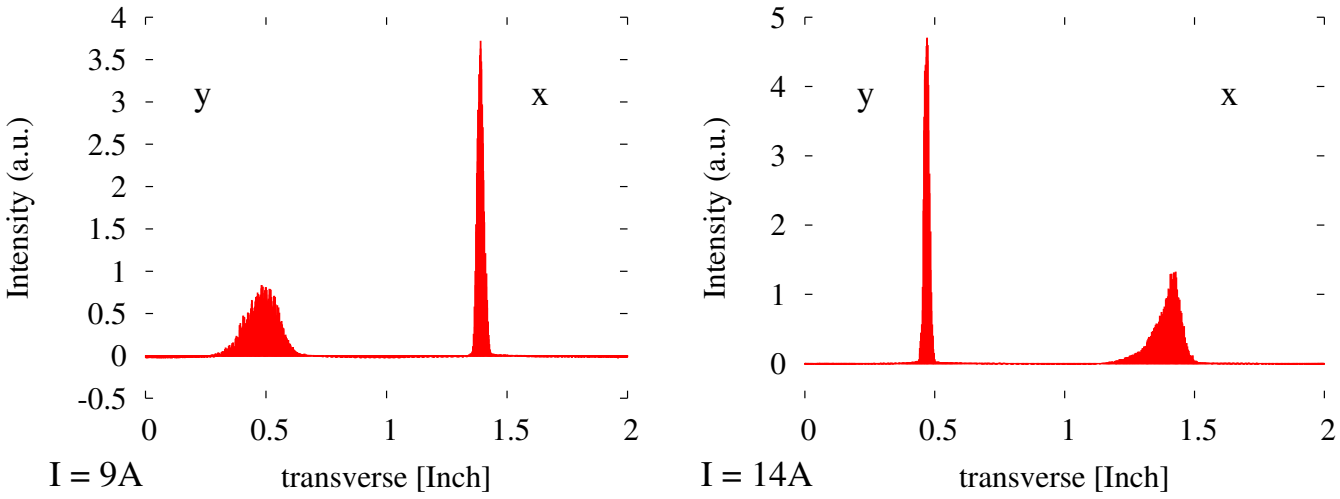

Figure 11: Sample of raw MEBT:RPM5 readings acquired on-line during June 2020 beam development using $^{20}Ne^{4+}$ from OLIS. The x (horizontal) and y (vertical) dimensions are labeled on the plot.

6.1 Skew-Gaussian Fitting MEBT:RPM5 Data

As the MEBT:RPM5 traces featured both skewness and noise, it was decided to attempt skew-Gaussian fitting to produce noise-free variants of the RPM data for MENT processing. This allowed for a comparison between processed and unprocessed datasets. The advantage of a skew-Gaussian over a regular Gaussian fit is to avoid systematically mis-estimating the centroid and variance. The skew-Gauss function possesses an asymmetry parameter α, whose sign determines the handedness of the skew. The skew-Gaussian used for this analysis is defined as:

$$s(x) = \frac{1}{\sigma\sqrt{2\pi}}\left(1 + \mathrm{erf}\left[\alpha\frac{(x-\mu)}{\sigma\sqrt{2}}\right]\right)\exp\left(-\frac{(x-\mu)^2}{2\sigma^2}\right) \tag{19}$$

The function erf refers to the Gaussian error function. The separated horizontal and vertical RPM datasets were fit using `scipy-optimize`. Select fits to MEBT:RPM5 data are presented in Figure 12. These fits were then used to generate MENT input files representing the measurements in a manner analogous to what was done in Section 5.

6.2 Reconstructed Distribution at MEBT:Q5

The on-line behavior of the tune was found to disagree with the tune assumption from [11], rendering the use of a plot featuring r_{ij} impossible (Fig. 5). Instead, as done in [3], the scans were defined by plotting the squared size of the beam size on the RPM. For these scans, the skew-Gaussian squared-variance parameter is plotted versus Q5 current in Figure 13. Two quadrupole scan sampling strategies were carried out, attempting to use the least possible amount of images supplied to MENT. First, sets of 3-datapoint scans was performed for each of x and y, in both cases including the minimum rms width RPM measurement. This was followed by 5-datapoint quadrupole scans, with added samples at $\pm$ 1A away from the minimum beam size setting. The quadrupole scan results are shown in Table 3. Each reconstruction was done with and without skew-Gaussian processing.

The reconstructed distributions in Table 3 are systematically larger for the raw RPM data compared to the skew-Gaussian datasets. A comparison of the MENT reconstructions for each of the reconstructions are shown in Figures 14 to 17. A comparison of reconstructed beam distributions for both of the processed and unprocessed 5-datapoint scans is shown in Figure 18. The unprocessed datasets resulted in streaking and filamentation, in addition to featuring longer low intensity tails which act to broaden to 2rms size of the reconstructed beam. It is unavoidable to conclude that the beam at the entrance of MEBT:Q5 does feature a low intensity tail which is prominent in the x-dimension. Ultimately, the skew-Gaussian fit acts to truncate this tail which reduces the 2rms sizes, though the fits preserve the core of the beam distribution, which is qualitatively similar in extent for both datasets in Figure 18.

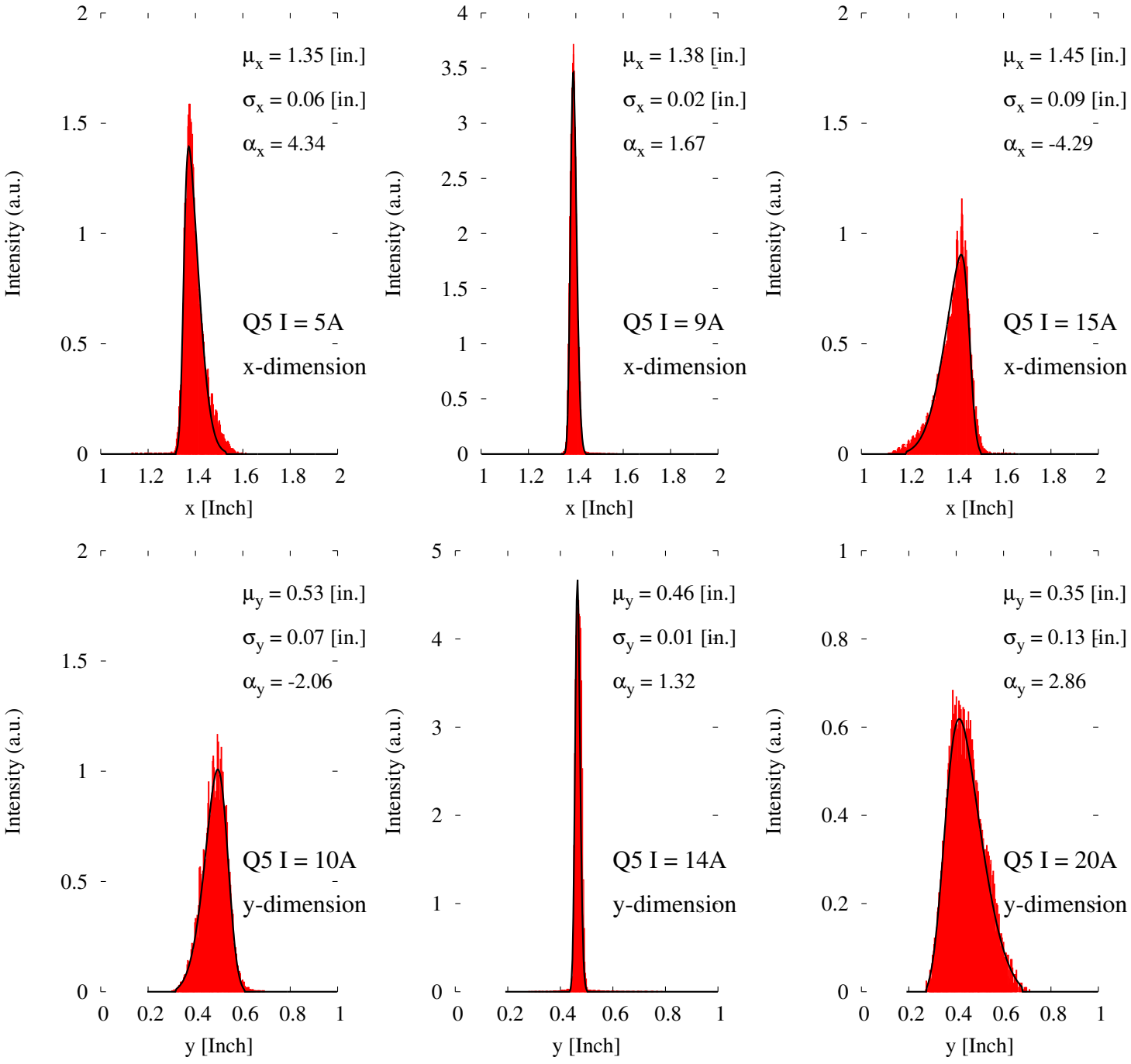

Figure 12: MEBT:RPM5 x (**Top**) and y (**Bottom**) raw data (red bars) and skew-Gaussian fit of Eq. (19) (black), along with fit parameters. Functions fit using `scipy_optimize`.

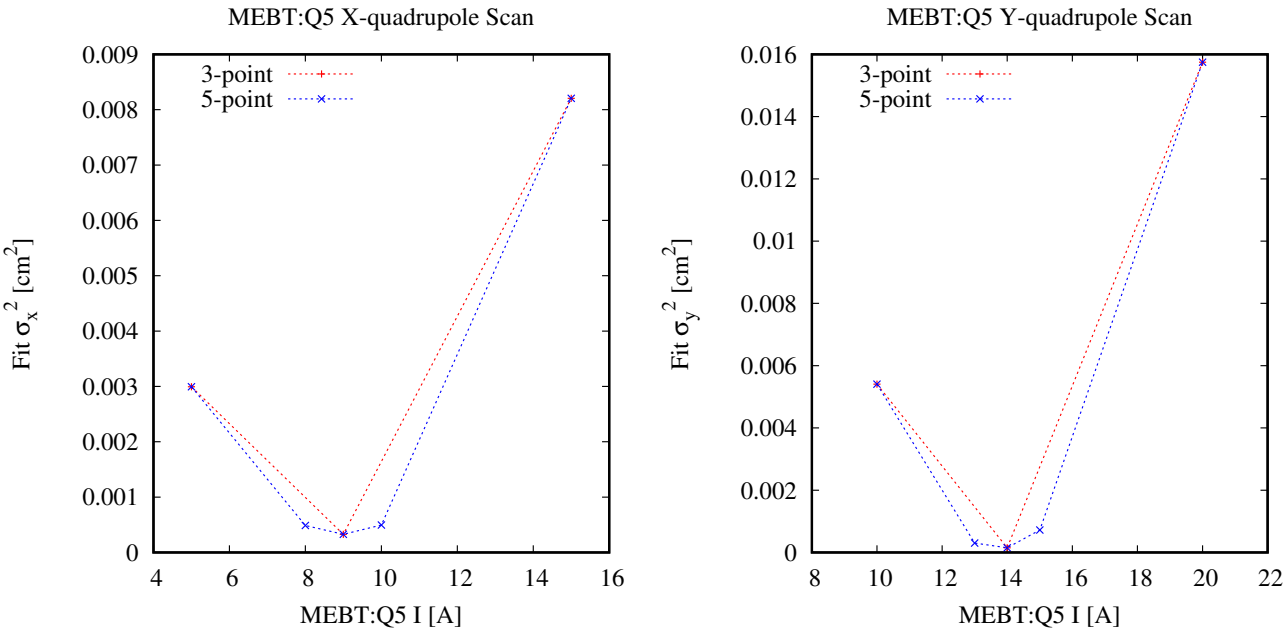

Figure 13: MEBT:RPM5 fit parameter σ^2 (Eq. 19) versus MEBT:Q5 current for x (**Left**) and (**Right**) y quadrupole scans from Table 3.

Dimension	Q5 I[A]	2xrms [mm]	2x'rms [mrad]	r_{ij}	ϵ_i [μm]	Fits	Scan
x (skewGauss)	(5,9,15)	3.97	11.76	-0.9939	5.16	Fig. 14, L.	Fig. 13, L.
x (unprocessed)	(5,9,15)	4.90	14.62	-0.9963	6.16	Fig. 14, R.	Fig. 13, L.
x (skewGauss)	(5,8,9,10,15)	4.04	11.92	-0.9935	5.50	Fig. 16, L.	Fig. 13, L.
x (unprocessed)	(5,8,9,10,15)	4.85	14.45	-0.9961	6.22	Fig. 16, R.	Fig. 13, L.
y (skewGauss)	(10,14,20)	5.55	6.30	0.9861	5.81	Fig. 15, L.	Fig. 13, R.
y (unprocessed)	(10,14,20)	5.41	6.30	0.9718	8.04	Fig. 15, R.	Fig. 13, R.
y (skewGauss)	(10,13,14,15,20)	5.54	6.29	0.9855	5.93	Fig. 17, L.	Fig. 13, R.
y (unprocessed)	(10,13,14,15,20)	5.47	6.39	0.9784	7.22	Fig. 17, R.	Fig. 13, R.

Table 3: Horizontal (x) and vertical (y) 3-datapoint quadrupole scan tomographic currents for MEBT:Q5, along with the resulting MENT reconstruction result for the beam distribution.

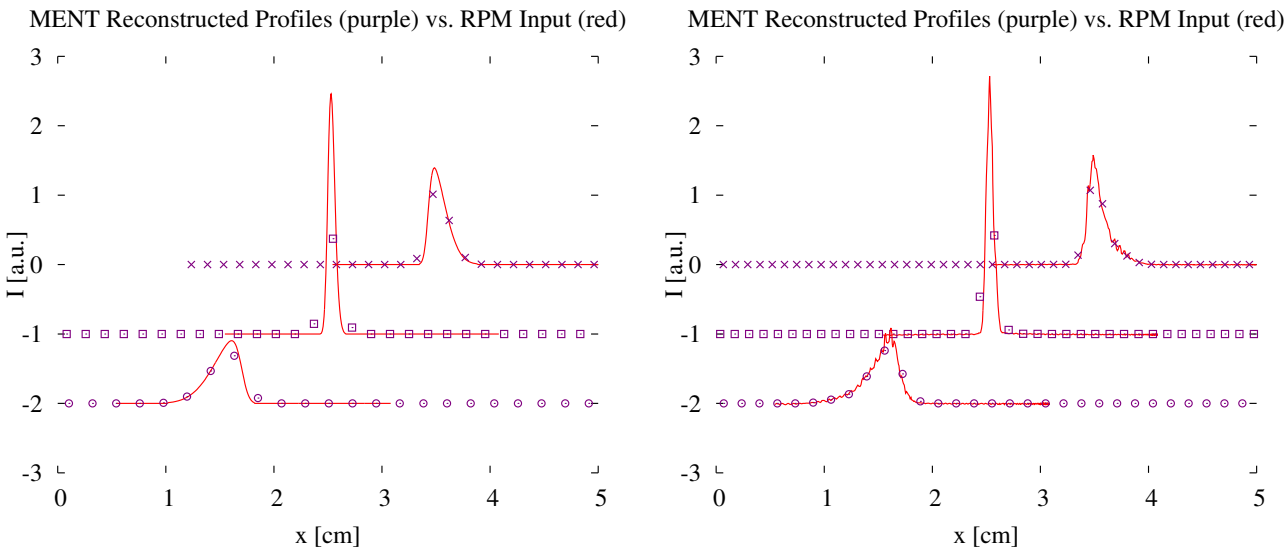

Figure 14: Comparison of MENT RPM profile reconstruction for skewGaussian data (**Left**) and unprocessed raw data (**Right**) for the x (horitontal) reconstruction.

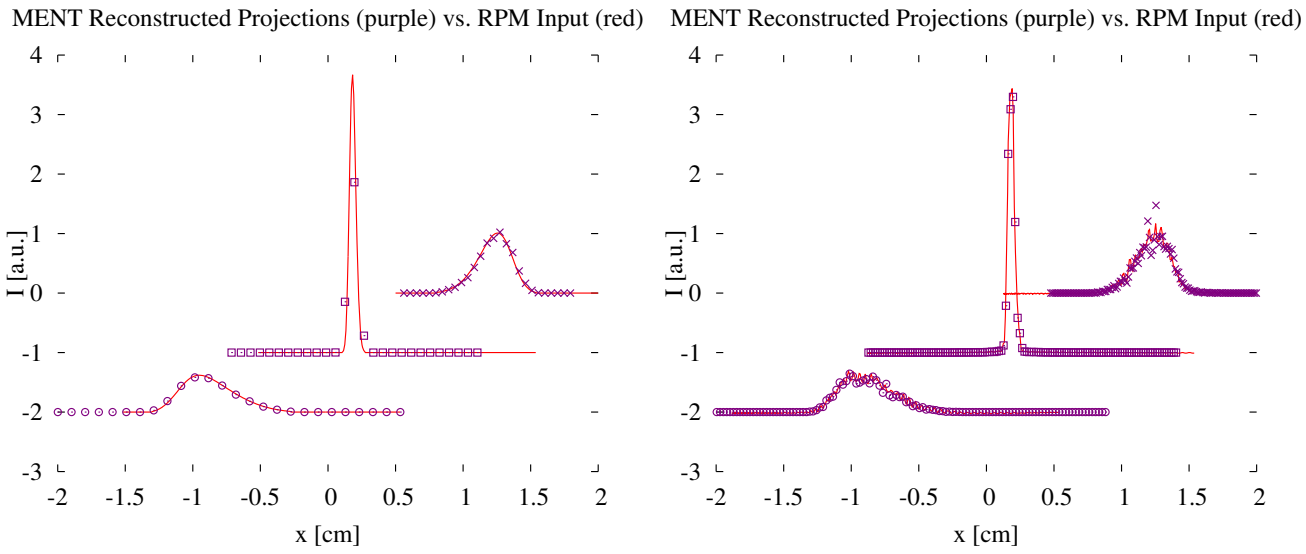

Figure 15: Comparison of MENT RPM profile reconstruction for skewGaussian data (**Left**) and unprocessed raw data (**Right**) for the y (vertical) reconstruction.

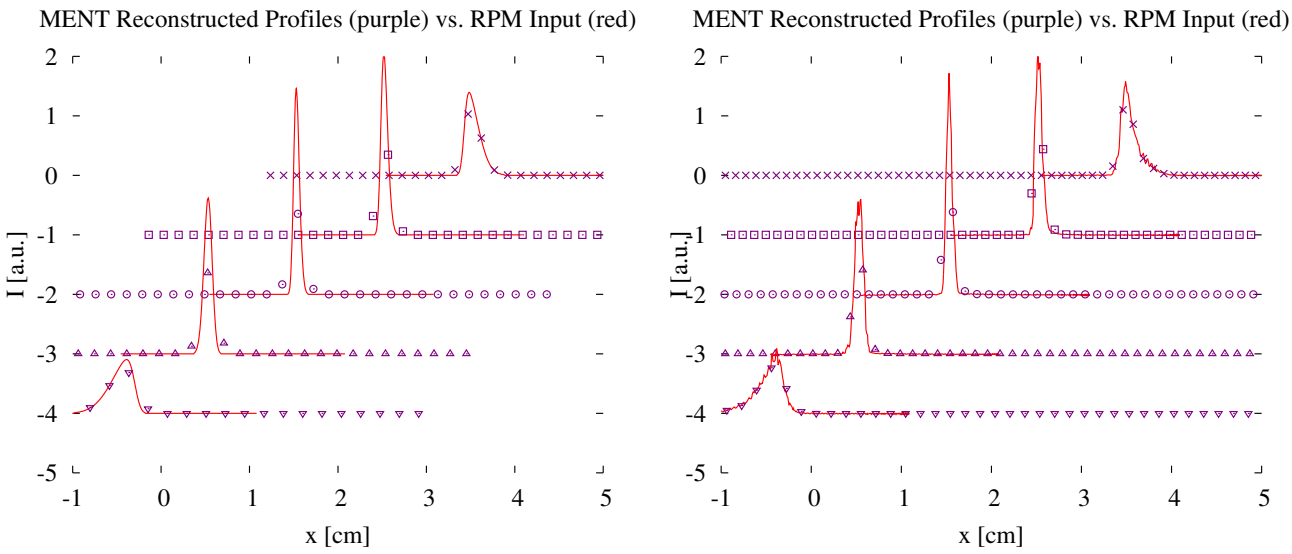

Figure 16: Comparison of MENT RPM profile reconstruction for skewGaussian data (**Left**) and unprocessed raw data (**Right**) for the x (horitontal) reconstruction.

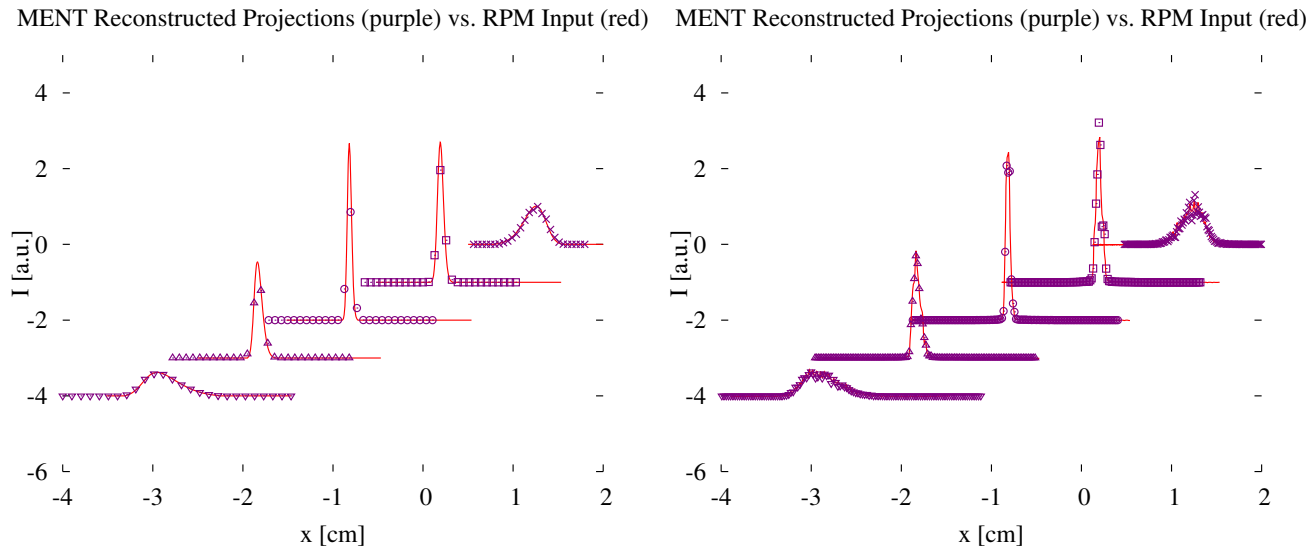

Figure 17: Comparison of MENT RPM profile reconstruction for skewGaussian data (**Left**) and unprocessed raw data (**Right**) for the y (vertical) reconstruction.

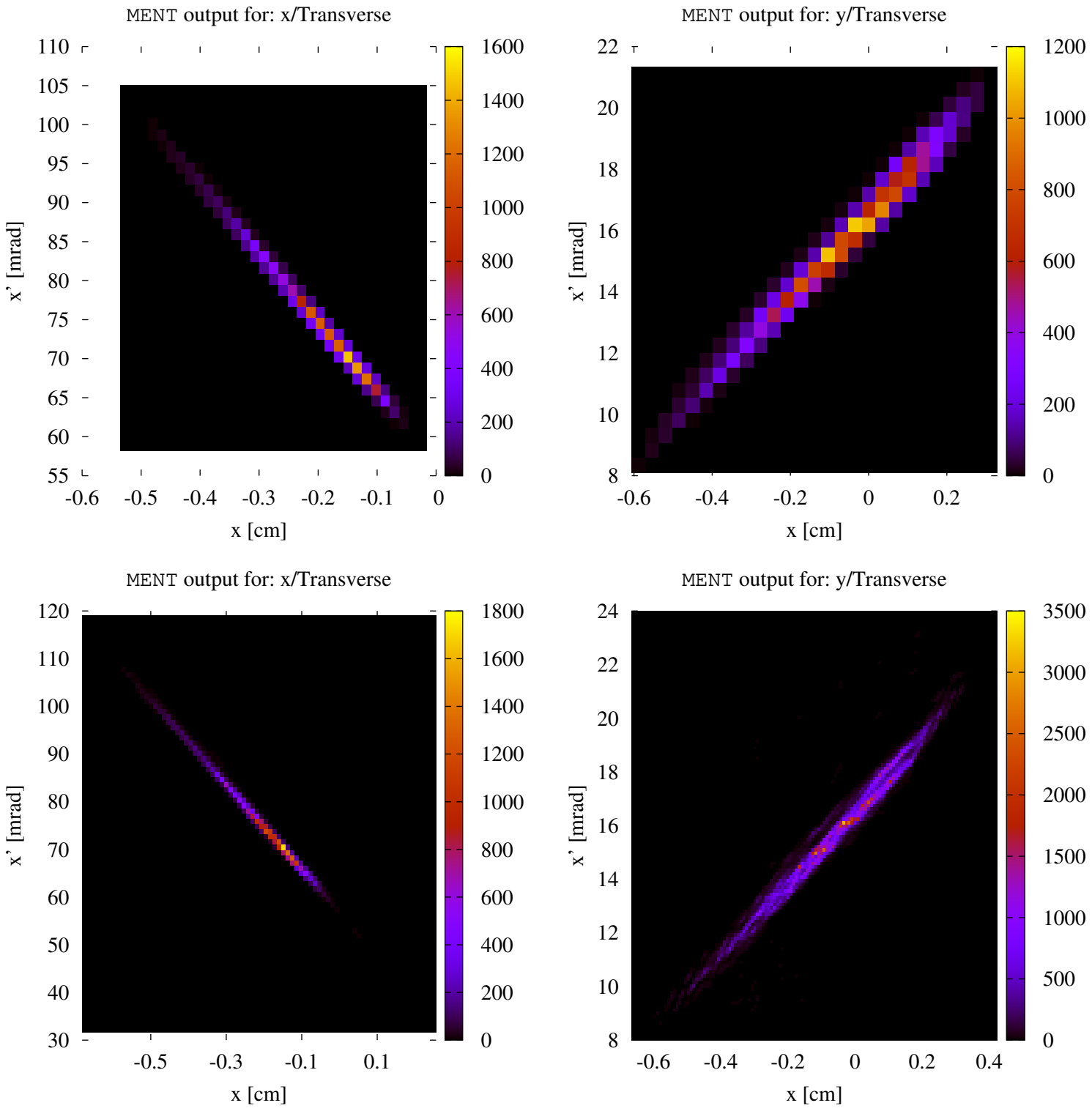

Figure 18: Skew-Gaussian processed 5-datapoint x (**Top-Left**) and y (**Top-Right**) quadrupole scan MENT reconstruction of beam distribution at entrance of MEBT:Q5. The same unprocessed reconstruction 5-datapoint x (**Bottom-Left**) and y (**Bottom-Right**) reconstructions, showing streaking and artifacts.

6.3 Back-Transported Distribution at ISAC-RFQ Exit

The matrix $\boldsymbol{\sigma_f}$ at MEBT:Q5 was transformed according to Equation (2) to the start of the `acc/` database sequence for the MEBT section, which coincides with the original `Trace3D` MEBT beamline simulation starting point [11]. This was repeated with each of the results from Table 3, producing a set of starting distributions $\boldsymbol{\sigma_i}$ located at the exit of the ISAC-RFQ. The resulting `TRANSOPTR` transverse beam envelopes from RFQ output to MEBT:RPM5 are shown in Figure 19. In all cases, the bunch rotator was manually tuned in `TRANSOPTR` to produce a time focus at the MEBT stripping foil. Moreover, the starting longitudinal RFQ beam distribution was taken from `PARMTEQ` simulations for a matched beam [17].

Source	Dimension	Skew-Gaussian?	2xrms [mm]	2x'rms [mrad]	ϵ_i [μm]	r_{ij}
3-pt.	x	Yes	3.81	5.06	3.94	0.9788
3-pt.	x	No	4.80	6.32	5.34	0.9844
5-pt.	x	Yes	3.70	4.94	4.02	0.9754
5-pt.	x	No	4.72	6.24	5.40	0.9831
3-pt.	y	Yes	2.48	5.32	5.14	-0.9213
3-pt.	y	No	2.48	5.43	8.13	-0.7969
5-pt.	y	Yes	2.47	5.34	5.26	-0.9174
5-pt.	y	No	2.51	5.31	7.29	-0.8365

Table 4: Reconstructed ISAC-RFQ output beam distribution using quadrupole scan MENT reconstruction, showing 3 and 5 datapoint quadrupole scans. Both skew-Gaussian processed and raw RPM data have been used. The effect of the bunch rotator is taken from the design tune in [11] and has not been measured online.

Each of the y datasets from Table 4 produce similar 2rms sizes for (y, P_y), though the correlation coefficient r_{34} is inconsistent. The x-datasets feature a consistent difference in size between raw and processed cases. The 2rms (x, P_x) sizes are greater for the unprocessed case, owing in large part to the prominent low intensity tail in the distribution. However, each x-reconstruction has a consistent value of r_{12}. Since the x-distribution is broad and skewed in configuration space, its size is sensitive to truncation though its correlation angle is not.

Each of the skew-Gaussian processed datasets in Table 4 feature a smaller emittance owing to this implicit truncation. Figures 20 and 21 show the reconstructed output RFQ transverse beam distributions for processed and unprocessed cases. The horizontal reconstruction prominently shows the effect of skew-Gaussian truncation on the low-intensity tail, while largely keeping the core of the beam distribution intact.

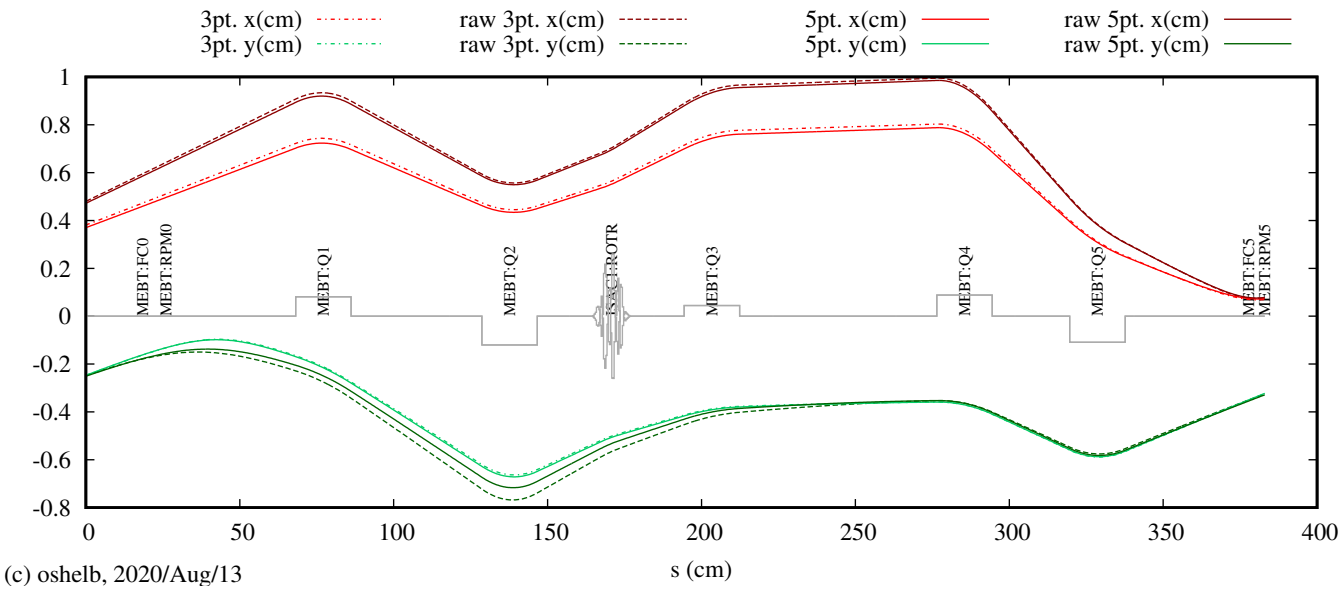

Figure 19: `TRANSOPTR` 2rms transverse envelopes from RFQ output to MEBT:RPM5, with the outlines of the 3-datapoint and 5-datapoint starting parameters from Table 4. x and y envelopes refer to 2xrms and 2yrms, respectively.

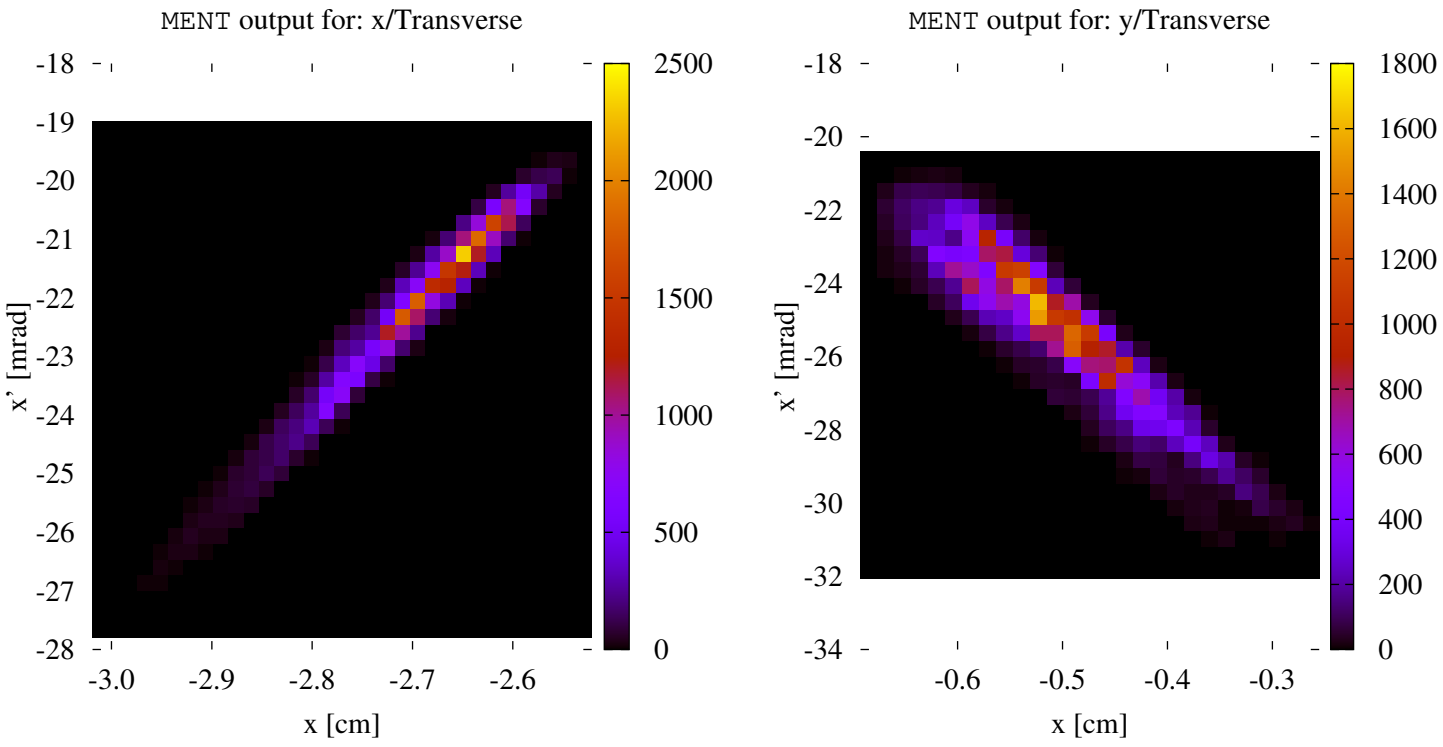

Figure 20: MENT reconstructions of skew-Gaussian processed 5-datapoint scans showing RFQ output (**Left**) x and (**Right**) y-distributions, prior to MEBT:Q1 at `acc/` database marker `start_t3d_mebt` [11].

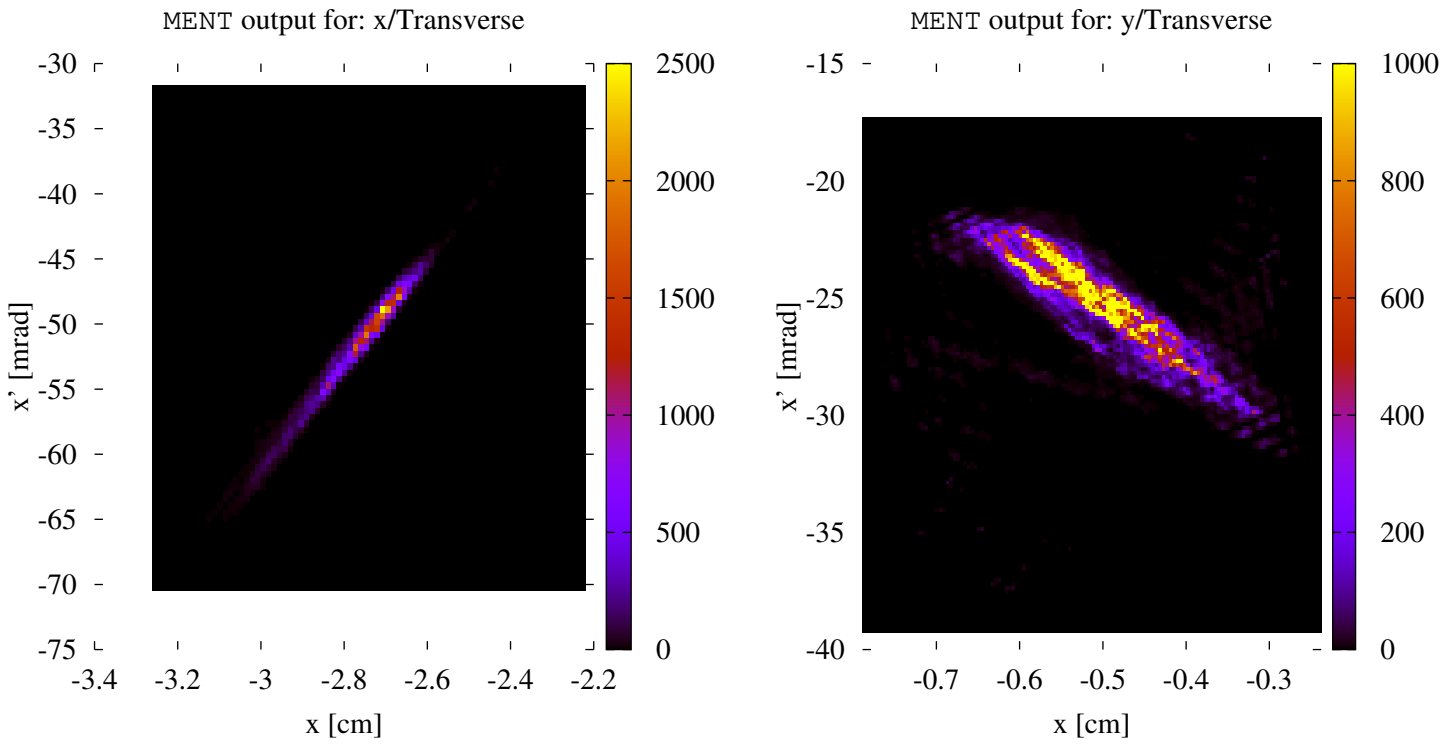

Figure 21: MENT reconstructions of skew-Gaussian processed 5-datapoint scans showing RFQ output (**Left**) x and (**Right**) y-distributions, prior to MEBT:Q1 at `acc/` database marker `start_t3d_mebt` [11].

6.4 Drifting the ISAC-DTL

As a final test of the MENT reconstructed ISAC-RFQ output beam distribution from Section 6.3, both of the 5-point distributions (processed and unprocessed) from Table 4 have been used to simulate the unaccelerated beam-envelope through the ISAC-DTL (E/A = 0.153 MeV/u), in `TRANSOPTR`. Both sets of envelopes are shown in Figure 22. During the development shifts, DTL transmission was measured as 89%. Available RPM measurements were only MEBT:RPM5 and HEBT:RPM5 as the slower linear position monitors in the DTL were not exercised. Nevertheless, the RPM traces have both been superimposed to the figure.

While it is clear that further intermediate diagnostic measurements are needed for a more thorough evaluation of tomographically reconstructed on-line beam simulations, the RPM traces shown in the figure are consistent with the `TRANSOPTR` computation.

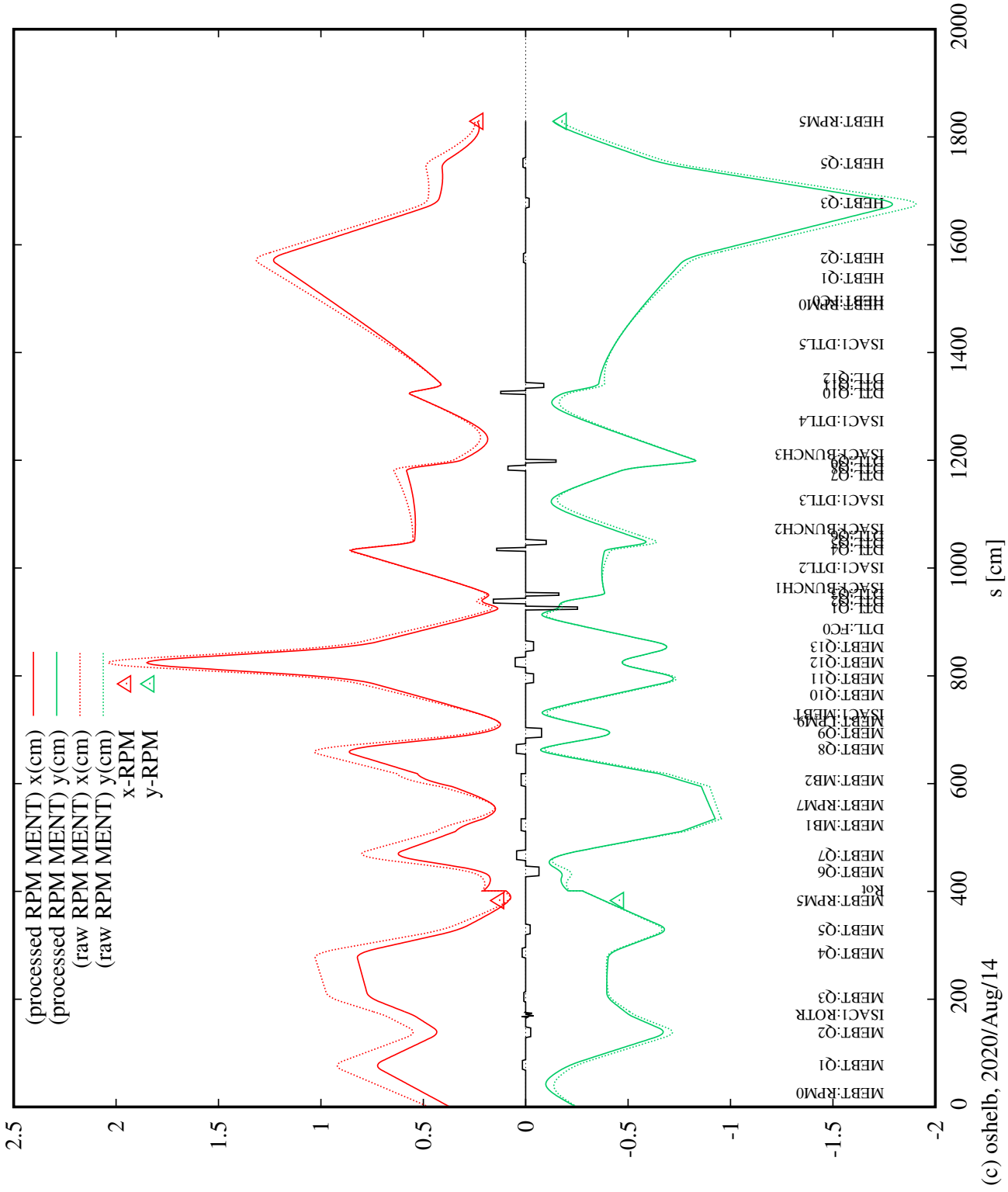

Figure 22: TRANSOPTR simulation of $^{20}Ne^{4+}$ beam from ISAC-RFQ exit, drifting the ISAC-DTL at E/A = 0.153 MeV/u showing 2rms containment envelopes. All quadrupole settings directly loaded from operational savetune. Normalized device transverse focal strengths are shown as a solid black line. Both processed (dotted) and unprocessed (solid) 5-datapoint MENT reconstructions from Table 4 were used for the computation.

7 Conclusion

In this report, MENT has been presented and explored using the beam envelope code `TRANSOPTR` and a plotting utility dubbed `twissify`. The latter proved very useful in producing simulated beam diagnostic traces, which were supplied to MENT as input data. This allowed for a dress rehearsal so to speak, enabling an exploratory simulation of a quadrupole scan tomography measurement at the output of the ISAC-RFQ, in the MEBT section. This was done using an envelope simulation that is known to approximate, but not exactly duplicate, on-line measurements. Insight was gained into conditions to avoid (non-monotonous $|r_{ij}|$ vs quad. current profile) and those to seek (scanning through a minimum waist) for successful measurements, free of artifacts.

An on-line quadrupole scan measurement was then performed using the MEBT Q5-RPM5 pair, downstream of the ISAC-RFQ. Beam consisted of $^{20}Ne^{4+}$ at an energy of 3.06 MeV (E/A = 0.153 keV/u). Smoothing was accomplished here by using a skew-Gaussian function to extract size parameters of the distribution. This enabled MENT reconstruction of the output RFQ transverse beam distribution, which is found to feature low intensity tails, with greater prominence in the horizontal (x) dimension. Further consideration should be given to the issue of noise handling and data processing for MENT.

8 Acknowledgements

The author wishes to thank members of the Beam Physics group for their patience and discussions. Yi-Nong Rao provided assistance and discussions regarding the use of the MENT routine. His work in the IMS section is also the first instance in which this technique was successfully carried out at ISAC and served as a strong reference for this work. Rick Baartman, Thomas Planche are thanked for their assistance and useful discussions. Oliver Kester has been the main driving force behind the deployment of quadrupole scan tomography at ISAC, and is thanked for his support. Spencer Kiy is also thanked for useful discussions, patience and for much of the web development work behind the nascent tomography HLA project at ISAC.

References

[1] YN Rao, R Baartman, and G Goh. Maximum-entropybased tomographic reconstruction of beam density distribution. *Proc. 2009 PAC, Vancouver, Canada*, 2009.

[2] YN Rao, R Baartman, et al. Transverse phase space tomography in triumf injection beamline. *Proceedings of IPAC2011, San Sebastian, Spain*, pages 1144–1146, 2011.

[3] Rao. YN. *Maximum Entropy Tomography Validation*. Technical Report TRI-BN-19-MENT, TRIUMF, 2019.

[4] S Saminathan, F Ames, R Baartman, M Marchetto, O Lailey, and A Mahon. Tomography reconstruction of beams extracted from an ion source. *Review of Scientific Instruments*, 90(12):123302, 2019.

[5] S Marcano. *Customizing Web Applications for Beam Tomography*. Technical Report TRI-BN-17-01, TRIUMF, 2017.

[6] D Tattan. On the beam tomography web application. Technical report, Tech. Rep. TRIBN-17-09, TRIUMF, 2017.

[7] Daniel Sehayek. Implementation of the phase space tomography algorithm. Technical Report TRI-BN-18-06, TRIUMF, 2018.

[8] Owen Lailey. Tomography Reconstruction for ARIEL CANREB Beam Commissioning. Technical Report TRI-BN-19-07, TRIUMF, 2019.

[9] Werner Joho. *Representation of beam ellipses for transport calculations*. Schweizerisches Institut für Nuklearforschung, 1980.

[10] Heighway EA and Hutcheon RM. *Transoptr - A second order beam transport design code with optimization and constraints*. Technical report, Atomic Energy of Canada Limited, 1981.

[11] Olivier Shelbaya. TRANSOPTR Implementation of the MEBT Beamline. Technical Report TRI-BN-19-02, TRIUMF, 2019.

[12] Olivier Shelbaya. The TRANSOPTR Model of the ISAC Drift Tube Linear Accelerator - Part I: Longitudinal Verification. Technical Report TRI-BN-20-08, TRIUMF, 2020.

[13] Olivier Shelbaya. TRANSOPTR Implementation of the HEBT Beamlines. Technical Report TRI-BN-19-06, TRIUMF, 2019.

[14] Gerald Minerbo. Ment: A maximum entropy algorithm for reconstructing a source from projection data. *Computer Graphics and Image Processing*, 10(1):48–68, 1979.

[15] Y.N. Rao. personal communication.

[16] Olivier Shelbaya and Richard Baartman. Langevin-Like DTL Triplet BI Fits and Analysis of Transverse DTL Tuning Difficulties. Technical Report TRI-BN-19-18, TRIUMF, 2019.

[17] O Shelbaya, R Baartman, and O Kester. Fast radio frequency quadrupole envelope computation for model based beam tuning. *Physical Review Accelerators and Beams*, 22(11):114602, 2019.

[18] Olivier Shelbaya. A Quick TRANSOPTR Primer. Technical Report TRI-BN-20-06, TRIUMF, 2020.

Appendices

A Twissify - A Python Companion to TRANSOPTR

twissify is a python based plotting package intended for use with the envelope code TRANSOPTR (optr) [10]. Specifically, it allows for the printing of ellipses representing the transverse beam distribution in optr. The code assumes optr has been run with the variable iprint set to -1 in data.dat. For a brief overview of running TRANSOPTR in such a manner, see [18].

A.1 Installation and Use

The script is intended for use on unix like systems. The files can be obtained by cloning them from gitlab [1]. Once this is done, for ease of use an alias can be defined, for example on a bash shell in the file /.bashrc:

```
alias twissify="python3 /path/where/twissify/gitcloned/twissify/twissify.py"
```

After sourcing the file or restarting the terminal, twissify can be executed straight from the command line. In the following example, the help flag has been used to print use options:

```
oshelb@oshelbx1:~$ twissify -h
usage: twissify.py [-h] [-a] [-s] [-m] [--marker MARKER] [-r] [-t] [--nolabel]

twissify: generate elliptical phase space beam distributions from TRANSOPTR
fort.envelope Olivier Shelbaya, TRIUMF Beam Physics Group, July 2020

optional arguments:
  -h, --help       show this help message and exit
  -a               animation (DEVELOPMENT)
  -s               start: print starting beam distribution (s = 0 cm)
  -m               menu: menu-based marker selection for plotting location
                   from fort.label
  --marker MARKER  marker: specify marker string - exactly as it appears in
                   fort.label
  -r               RPM: output synthetic/simulated Gaussian RPM traces for x/y
  -t               tomography: MENT-compatible transfer matrix followed by
                   simulated Gaussian RPM trace (use to assemble MENT input
```

[1] contact me for a link to the gitlab repository if interested!

```
                file)
  --nolabel     disable all output labels on output ellipse graphs (other
                than axis ticks/labels/units)
```

To successfully run `twissify`, first change directories into the desired working `TRANSOPTR` folder. Then, simply call `twissify` from the command line with the desired flags. The script will read `fort.label` and `fort.envelope` in the current directory and produce the desired output in a new folder `twissify/`, in the same working directory. The transverse ellipses are stored as filenames `ellipsx.eps` and `ellipsy.eps`, while simulated RPM readbacks (if desired) are saved as `rpmx.dat` and `rpmy.dat`.

Calling `twissify` without markers will print the transverse trace space ellipses at the end of the file `fort.envelope`. Further note that calling the program with the marker `--nolabel` will disable all labeling on the output ellipse graphs, except axis units and tick labels. All other information won't be displayed.

A.2 Menu Based Marker Selection

The flag `-m` displays a menu showing each marker, as it is read from `fort.label`, with the associated optr s-coordinate. The user then types in the marker name at which location it is desired to print out the transverse configuration space ellipses. Note that the marker title must be entered exactly as displayed.

A.3 Rotary Position Monitor Spoofing

Using flag `-r` will generate two Gaussian distributions generated from the second moments in `fort.envelope`, at the specified printing location. Note that the RPM implementation is at present unique, though the code can easily be expanded to cover other diagnostic device types in a similar way. Should such additions be made, this document will be revised accordingly.

A.4 Marker Specific Selection

The combination `--marker` [STRING] can be used directly from the command line, if the marker corresponding to the s-location of the ellipse is known. An example use with a marker from the ISAC MEBT section (Faraday cup 5) consists of:

```
twissify --marker MEBT:FC5 -r
```

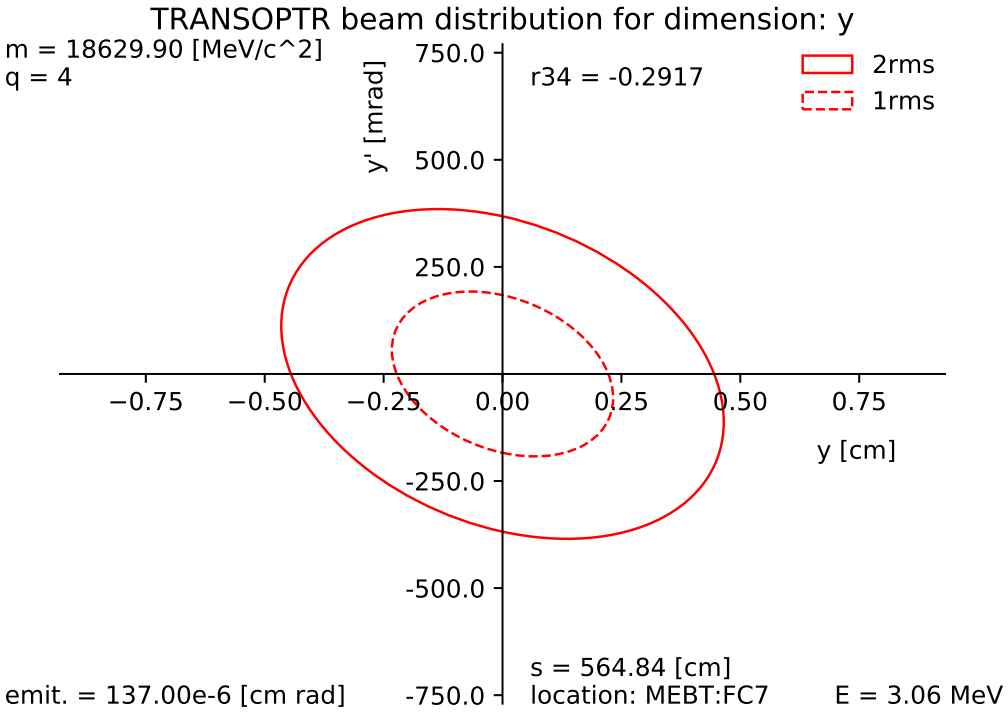

Figure 23: .eps output file produced by `twissify`, showing the different parameters as read-in from the `TRANSOPTR` files `data.dat`, `fort.label` and `fort.envelope`. The solid red ellipse delineates the 2rms containment boundary, while the dotted line contains 1rms of the beam distribution.

we further note that the marker `-r` was also used, which will print the corresponding transverse beam envelope at MEBT:FC5 *were there to be an RPM measurement made at that location.*

A.5 Tomographic Input File Spoofing (MENT)

The flag `-t` (which forces flag `-r` true) enables RPM spoofing, however the files `rpmx.dat` and `rpmy.dat` are formatted as a single entry of a Maximum Entropy Tomography reconstruction algorithm (MENT), as is used for beam based tomographic reconstruction at TRIUMF. This allows the user to sequentially run `TRANSOPTR` while iterating a quadrupole setpoint, produce a simulated beam distribution at a specified location downstream and build a synthetic MENT input file. This functionality has been developed to render less laborious the generation of calibration data for the

MENT algorithm as presently used.

A.6 Animation

Using the flag `-a` will prompt the user for a few desired parameters such as starting and ending location, animation quality and number of frames, producing a .gif animation file in the folder `twissify/`.

A.7 Use Example: Generating a Synthetic MENT Input File

In this example, I generated a `TRANSOPTR` sy.f/data.dat combo from the `acc/` database, representing a segment starting at the beginning of MEBT:Q5 and terminating at MEBT:RPM5, the downstream rotary position monitor. The goal of this exercise is to create a simulated input file for the maximum entropy tomographic reconstruction algorithm (Ment) [14]. The input file structure for the algorithm consists of the four elements of the (x,x') or (y,y') transfer matrix, from the start of sequence to the RPM.

Using `twissify -t` will grab the relevant m_{ij} elements from `fort.envelope`, which represent the point-to-point transfer matrix elements from the start of the `sy.f` file, up to the location from which they are extracted. This is always true for `twissify`. Thus, for use in MENT reconstruction, the `sy.f` file must always start at the desired location of tomographic reconstruction.

Since in this case `sy.f` only runs from the desired reconstruction point (just before MEBT:Q5) up to MEBT:RPM5, one can obtain the requisite building block of the MENT file by calling:

```
twissify -t
```

Then, in the folder `twissify/`, the files `rpmx.dat`, `rpmy.dat` are both structured as follow:

```
/
 0.50800872  23.47231670
-0.04312266  -1.00821900

 0.0000 0.0000
 0.0025 0.0000
 0.0051 0.0000
 0.0076 0.0000
 0.0102 0.0000
 0.0127 0.0000
 0.0153 0.0000
```

```
0.0178 0.0000
0.0203 0.0000
0.0229 0.0000
0.0254 0.0000
0.0280 0.0000
0.0305 0.0000
0.0331 0.0000
0.0356 0.0000
...
```

The first column represents the position in centimeters while the second column represents the intensity, for a standard Gaussian distribution of the form:

$$I(x) = \frac{1}{\sigma\sqrt{2\pi}} \exp(-\frac{(x-\mu)^2}{2\sigma^2}) \tag{20}$$

where the parameters σ are related to the `TRANSOPTR` output via:

$$\sigma = \frac{(2xrms)}{2} \tag{21}$$

similarly for y, where in either case the value (2xrms) is directly read in from `fort.envelope`.

Since the output is associated with a single `TRANSOPTR` run for which MEBT:Q5 was set to a single value, it is necessary to generate supplemental simulated MENT RPM input blocks as shown in red above, but for other values of the quadrupole. This is exactly analogous to an operator needing to scan the RPM at different quadrupole settings to perform on-line quadrupole scan tomography. This also means that one must ensure that the 2rms width of the beam at the RPM is iterated through a minimum.

Before changing the quadrupole value in `data.dat` and running `optr` from the command line, we begin assembly of the MENT input file:

```
cat twissify/rpmx.dat >> spoof_x.dat
```

Note that we have placed the MENT input file in the main optr folder itself and not the `twissify/` folder, as it is overwritten at each execution of `twissify`. Assuming the first iteration had MEBT:Q5 at say, 5A, and that for this hypothetical sequence we wish to simulate a 5A to 15A sweep, with 1A step size, we change MEBT:Q5 current from 5A to 6A in `data.dat`, and run `TRANSOPTR` from the terminal once more. With the second iteration of optr complete, we once more run `twissify` to produce another component of the MENT input file:

```
twissify -t
cat twissify/rpmx.dat >> spoof_x.dat
```

as we're appending to the MENT file, it now contains transfer matrices and (simulated, Gaussian) x-RPM traces for MEBT:Q5 set at 5 and 6 amps. To complete the sequence, the above is re-iterated (manually or by scripting) until the simulated measurement is complete, at MEBT:Q5 I = 15A.

Since MENT expects the very first line of the input datafile to be the first two transfer matrix elements and not the forward slash, we remove line-1 from the file `spoof_x.dat`:

```
sed -i '2d' spoof_x.dat
```

The simulated MENT file can now be used in `MENT`, coupled for example with the following `in` file:

```
INPUT: ./spoof_x.dat
MAX ITERATIONS: 50
INTERPOLATE N: 100
SMOOTH FACTOR: -1
CONTOUR START: 0.100
CONTOUR END: 0.900
```

One now has in hand both the input file `in` and the data file `spoof_x.dat`, which can be used to perform tomographic reconstruction of the beam distribution, based on simulated data from `TRANSOPTR`.

Such an example was performed using a $^{20}Ne^{4+}$ beam with (x,x',r12) = (0.2cm, 5mrad,-0.99) in `TRANSOPTR`, simulated in the ISAC-MEBT section [11]. Sequential use of `twissify -t` on an optr system file including MEBT:Q5 allowed for the easy generation of simulated traces on the downstream rotary position monitor, MEBT:RPM5. The MENT input file was put together following the above discussed procedure, and MENT was then run, with the output shown in Figure 24. The reconstruction is only qualitatively presented in this work, with a more thorough investigation using `twissify` in this manner underway separately.

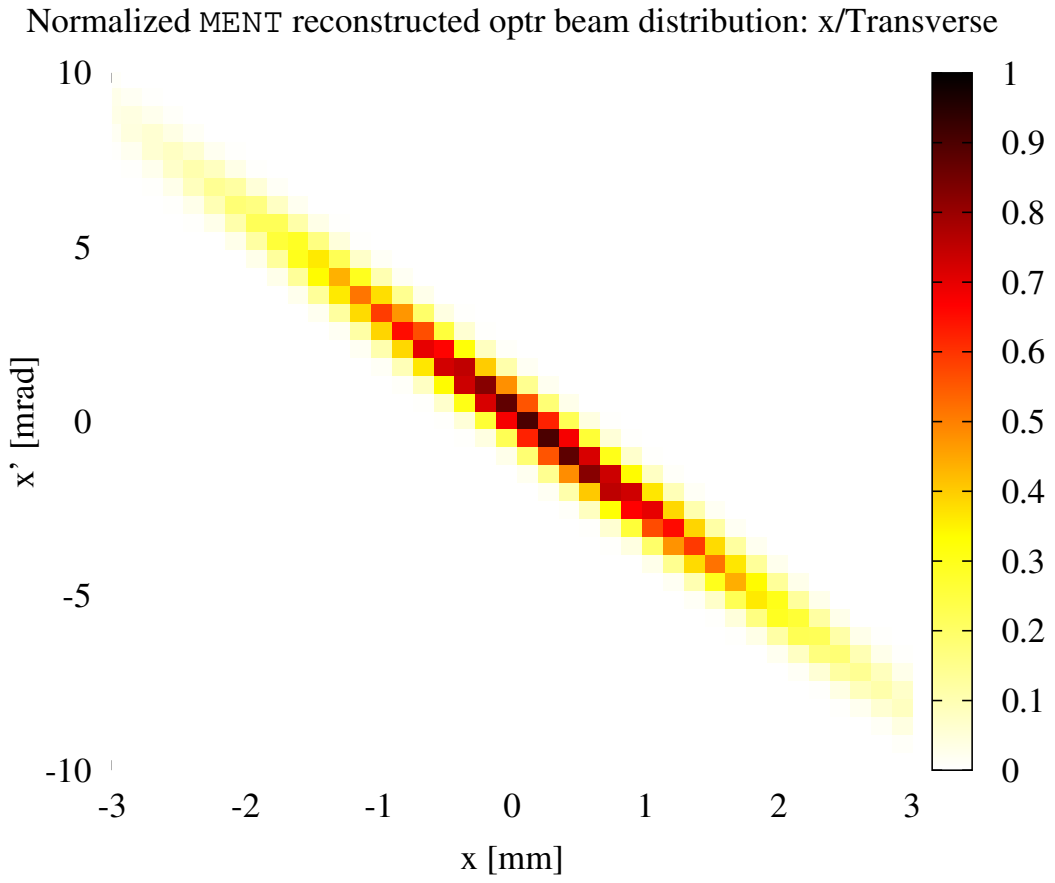

Figure 24: Using `twissify`, a simulated quadrupole scan tomography measurement was performed using a `TRANSOPTR` generated E = 3.06 MeV, $^{20}Ne^{4+}$ ISAC-RFQ output beam. The flag `-t` was used on an `sy.f` file starting at the entrance of MEBT:Q5 and terminating at MEBT:RPM5, the simulated diagnostic device. This allowed the generation of a synthetic MENT input file, which was used to tomographically reconstruct the initial beam distribution. In this case, the starting `TRANSOPTR` parameters were (x,x',r12) = (0.2cm, 5mrad,-0.99).